Journal of Materials Science Research and Reviews

2(2): 258-282, 2019; Article no.JMSRR.47734

Effect of Different Annealing Temperatures on Structural, Optical, Morphological and Electrical Properties of Cu - ZnO Thin Films Prepared Using Sol—gel Spin Coating Techniques

Mohana F. Attia[1*]

[1]Department of Mechanical Engineering - Physics, Alasala Colleges, College of Engineering, P.O.Box 2666, Dammam 31483, Saudi Arabia.

Author's contribution

The sole author designed, analysed, interpreted and prepared the manuscript.

Article Information

Editor(s):
(1) Dr. Madogni Vianou Irenee, Departement de Physique, Laboratoire de Physique du Rayonnement LPR,Cotonou, Universite d'Abomey-Calavi (UAC), Benin.
Reviewers:
(1) Yuan-Tsung Chen, Graduate School of Materials Science, National Yunlin University of Science and Technology, Taiwan.
(2) Kasem K. Kasem, Indiana University Kokomo, USA.
Complete Peer review History: http://www.sdiarticle3.com/review-history/47734

Original Research Article

Received 26 December 2018
Accepted 05 March 2019
Published 01 June 2019

ABSTRACT

In this study, Cu - doped ZnO thin films were prepared at different annealing temperatures from Copper acetate precursor by sol-gel spin coating method for Photocatalytic Applications. The films were characterized by X-ray diffractometer (XRD), scanning electron microscopy (SEM), and Fourier transform infrared spectroscopy (FTIR). The obtained powders were annealed under air in the range of $T_c = 250^0 - 550^0\ C$, for Cu – ZnO. The surface morphological, structural, electrical and optical properties of the as-deposited ZnO films have been investigated as a function of Cu-doping level. The thickness of the films was estimated by Fizeau fringes interference method which varied from 195 to 198 nm. The X-ray diffraction analysis indicated that the wurtzite structure was maintained for all samples and copper was successfully doped into ZnO at low T_C. However, the formation of monoclinic CuO was observed at higher T_C. For Cu – ZnO, the crystallite size increased with the annealing temperature from 15.86 to 24.24 nm. The isotherms obtained were type IV with a hysteresis type H 3, confirming the mesoporous behavior of the catalysts. The surface area was in the range of 35.1 to 8.66 m^2/g. All the prepared catalysts mainly showed two emission regions: a sharp peak in the ultraviolet region and another broad peak in the visible

**Corresponding author: Email: mohana.attia@alasala.edu.sa;*

region. The photocatalytic activity was achieved by the degradation of 300 mg/L malachite green (MG) aqueous solution under UV irradiation. The findings showed that the increased annealing of different concentration of Cu doped ZnO with CuO on the surface resulted in highly improved photocatalytic activity. Various optical constants such as absorbance, transmittance of the films have been studied. The values of transmittance are high in the visible and IR region and it is minimum in the UV region. Absorbance decreases with higher percentage of Cu concentration. The band gap of the films varied 3.21 to 3.05 eV. The resistivity gradually decreases with the increase of temperature, which indicates the semiconducting nature of the materials. Resistivity also increases with the increasing doping concentration. The conductivity decreases with the increasing of Cu concentration.

Keywords: Zinc oxide; sol – gel; malachite green; annealing temperature; copper; photocatalytic activity; resistivity; conductivity.

1. INTRODUCTION

Nanotechnology can be better demonstrated by the technology of design and applications of nanomaterials. Nanoscale oxides of transition metals are of most significance for several applications in optoelectronics [1]. The most emerging technology in today's world is Transparent Electronics through which wide bandgap semiconductors are applied in applications of optoelectronic devices [2] and potent exciting binding energy of 60 meV [3]. Also, Nanoscale Oxides has other important application such as solar cell, gas sensor, Li-ion batteries, supercapacitors [4]. The important advantages of ZnO include its ability to absorb large quantity of visible light than TiO_2, environmental sustainability, its low cost and high catalytic efficiency. For this reason, ZnO is suitable and more effective in the photocatalytic degradation of some dyes. ZnO crystallizes in a hexagonal wurtzite structure with the lattice parameters of (c = 5.205 Å, a = 3.249 Å) [5]. Doping ZnO with a transition metal such as Cu [6] has been verified as an effective method to adjust its functionality including electrical and optical properties Cu-doped ZnO has shown significantly improved properties such as electrical, magnetic, photocatalytic performance and gas sensing properties. In practice, ZnO-based thin films can be grown by diverse growth techniques including radio frequency magnetron sputtering (RFMS), pulsed laser deposition (PLD), laser molecular beam epitaxy (P-MBE) [6], spray pyrolysis [7], metal organic chemical vapour deposition (MOCVD) [8], and sol-gel spin coating method [9]. Among these methods, spin coating can provide the ease of chemical composition of doping, which is an advantage over the others. Annealing and doping are important approaches used to improve ZnO as a photocatalyst and are more effective and play important roles in controlling the intrinsic defects of ZnO. Moreover, annealing increases the crystallinity of ZnO, decreases the defect on its surface, and reduces its band gap energy. Radiation handling of polymers is a non-power application and at most consists of cross linking, curing, grafting, and degradation. Ion beam irradiation is a well decided tool for the modification of polymer surfaces, useful for controlled changes of a variety of characteristics, like chemical reactivity, hardness, wear [10-13]. In the present work, Nanocrystalline thin films are prepared by simple, low-cost sol-gel spin coating technique, and the effect of different annealing temperatures on structural, optical, morphological and electrical properties of the films are investigated for Photocatalytic Applications. The attraction can simply be attributed to the large exciton binding energy of 60 meV of ZnO potentially paving the way for efficient room-temperature exciton-based emitters, and sharp transitions facilitating very low threshold semiconductor lasers [14-18]. ZnO is a low-cost, ecofriendly, and versatile material to be used to generate emission colors all over the rainbow spectrum. The reason for the color tuning is the band edge emission as well as the different defect related emissions. The defect related emission in ZnO is dependent on the synthesis method, annealing temperature, and several other parameters [19]. The nanostructure tailoring of ZnO is dependent on growth conditions and doping concentrations. ZnO nanostructures have attracted a great attention as optical components in nanometer sized electronic devices due to the enhanced quantum confinement effect and high surface to volume ratio [20-22]. Zinc oxide (ZnO) is a technologically useful material due to its wide band gap of 3.37 eV. Furthermore, ZnO has other advantages such as high chemical and physical stability, thermal stability in hydrogen

plasma atmosphere, large exciton binding energy of 60 meV [23-25].

2. EXPERIMENTAL SECTION

2.1 Synthesis of ZnO and Cu- doped ZnO Nanoparticles

Zinc acetate dihydrate [Zn $(CH_3\ COO)_2\ .2H_2O$], absolute methanol, tartaric acid $(CHOH\text{-}COOH)_2$, Copper nitrate trihydrate [$Cu(NO_3)_2\ .3H_2O$] and malachite green (MG) were purchased from Sigma-Aldrich. All chemicals were utilized without further purification. Double distilled water was used in all solution preparations. Cu – doped ZnO thin films were prepared by sol-gel method using zinc acetate dehydrate $(CH_3\ COO)_2\ Zn{\cdot}2H_2O$ and Copper acetate dihydrate $Cu_3[(CH_3\ COO)_2{\cdot}H_2O]$ as starting precursors. The 2-methoxy ethanol ($C_3H_8O_2$) and diethanal amine (DEA) were selected as the solvent (0.5 M, 100 mL) and sol stabilizer, respectively. The prepared mixture was vigorously stirred at 100°C for 5 h by magnetic stirrer and cooled to room temperature for 24 h. The precursors prepared at different copper concentration of 2-20 wt.% were spin-coated on borosilicate substrates at room temperature with speed of 3000 rpm for 30 s. After repeating the coating procedure 6-times, all coated films were annealed at various temperatures ranging from 550^0C for 3 h in ambient air.

2.2 Materials Characterization

The morphology of the nanopowder samples was examined using a scanning electron microscope. The samples were previously oven dried and coated with a thin film of gold to provide ZnO powder surface with electrical conduction. The composition and average size of nanoparticles were determined by the powder X-ray diffraction patterns, the samples were recorded by a diffractometer (Bruker D8 – Advance), measurements were performed to identify the structural properties and crystalline behavior of the films using Cu-Kα radiation (λ =0.15406 nm). The accelerating voltage and scanning angle were 40 kV and 20^0 –75^0c, respectively. The mode of chemical bonding in the prepared samples was studied by Fourier transform infrared spectroscopy (Model: Nicolet 6700) in the range 4000–400 cm^{-1} with a resolution of 4 cm^{-1}. The surface area and pore sizes of nanoparticles were determined by the Brunauer–Emmett–Teller (BET) method (aims to explain the physical adsorption of gas molecules on a solid surface and serves as the basis for an important analysis technique for the measurement of the specific surface area of materials) using a Micrometrics ASAP 202 apparatus (degas temperature: ambient to 200^0C for 20 min with pressure range of 0 to 950 mmHg). The optical measurements of the Cu – doped ZnO thin films were carried out at room temperature using spectrophotometer [Labomed – UVS 2800] in the wavelength range of 190 nm to 1100 nm. Room temperature photoluminescence studies were carried out using the (Perkin Elmer LS55 Luminescence).

2.3 Determination of Heterogeneous Photocatalytic Activity

The photoactivity of prepared ZnO and Cu-doped ZnO were examined using (MG) dye as a pollutant and all experiments were carried out in a Pyrex photoreactor under UV irradiation. After achieving adsorption equilibrium in the dark, the solution was illuminated for photocatalytic kinetic study: The samples of the MG solution were taken after different irradiation times and were analysed using UV–visible spectroscopy at a wavelength max=618 nm. Using the Beer-Lambert law, the absorption measurement was converted to concentration. The photocatalytic degradation efficiency was calculated using the following equation: [26-27],

$$Mg\ \% = [(C_0 - C_t)/C_0] \times 100\% \quad (1)$$

Where $\boldsymbol{C_0}$ is the [MG] initial concentration, and $\boldsymbol{C_t}$ is the [MG] concentration at time $\boldsymbol{t}$.

2.4 Film Thickness

The film thicknesses of Cu- ZnO thin films were measured by the Fizeau fringes method in the department of Physics. The thickness of the film "d" can then be determined by the relation:

$$d = \frac{\lambda}{2}\frac{a}{b} \quad (2)$$

Where, λ is the wavelength and $\frac{a}{b}$ is the fractional discontinuity. In general, the sodium light is used, for which λ = 5893 Á. In conclusion, it might be mentioned that the Tolansky method of film-thickness measurement is the most widely used and in many respects also the most accurate and satisfactory one [28-29]. The thickness of the films was estimated by Fizeau fringes interference method which varied from 195 to 198 nm.

3. RESULTS AND DISCUSSION

3.1 Scanning Electron Microscopy Image (SEM)

The SEM micrographs of ZnO and Cu - ZnO annealed at 550^0C was shown in Fig. 1. The particles of the obtained powder were spherical in shape with a little agglomeration. Table 1 shows the weight percentages of the elements.

It was clearly observed that both films have a smooth surface comprising uniform grain size. As the annealing temperature increases, the crystalline structure and grain size of the film improves. The morphology of the 20 wt. % CZO show mixtures of Nanocrystalline CZO grains and a big number of other granular particles which may be CuO particle due to redundant Cu doping. This characteristic suggested the limitation of Cu doped on ZnO film. The random tendency of grains and the uneven surface may be related to the growth being along different crystal orientation.

3.2 Characterization of the Prepared Catalysts by X-ray Diffraction (XRD)

The structural properties of annealed ZnO and Cu-doped ZnO films on glass substrates are investigated by X-ray diffraction patterns. XRD patterns of ZnO and Cu doped ZnO films at various concentrations are shown in Fig. 2. The results show broad peaks at positions 31.61^0, 34.39^0, 36.11^0, 47.40^0, 56.52^0, 62.72^0, 66.29^0, 67.91^0 and 69.08^0 of the spectra. These values are in good agreement with the standard card file (JCPDS 36-1451) for ZnO and can be indexed as the hexagonal wurtzite structure. In addition, the appearance of a very low-intensity diffraction peak at position 38.65^0, corresponding to CuO as the monoclinic (base-centered) phase (JCPDS# 18-1916) was observed. The appearance of this peak is due to the high quantity of doped Cu and can be detected by XRD. The average crystallite size (D) of the prepared nanomaterial shown in Table 2 was calculated using Scherrer's equation: [30],

$$D = \frac{(0.9\,\lambda)}{(\beta\cos\theta)} \quad (3)$$

Where, ***D*** is the grain diameter, ***λ*** is the X-ray wavelength of Cu Kα (0.154 nm), ***β*** is the full-width at half maximum (FWHM) and ***θ*** is the Bragg angle [31].

The intense peaks in the XRD pattern of all samples clearly show the information of the hexagonal wurtzite phase of ZnO having prominent (002) plane in all samples, which is the most stable phase of ZnO. The shift in the (002) peak for higher Cu concentrations might be the substitution of Zn by Cu in the hexagonal lattice. The effect of Cu doping can be observed at the same annealing temperature ($T_C = 550^0$ C) as shown in Fig. 2. In comparison with ZnO, the introduction of copper ions shifted the diffraction peaks to higher angles by 0.060. Indeed, this change can be attributed to the replacement of Zn ions (ionic radii = 0.60 A) by Cu ions (ionic radii = 0.57 A) or may be due to structural stresses and modification of the lattice parameters of ZnO. This shift value indicated a decrease in the lattice parameters since the value of c parameter decreased by about 0.01 A from undoped ZnO (5.226 A) to Cu-doped ZnO (5.217 A). This decrease confirmed that the substitution of Zn ions by Cu in the ZnO lattice, was facilitated by the similarity of the ionic radii. Sharma et al. [32], in their study on Mn-doped ZnO, reported similar observations.

Table 1. Weight percentage of the elements obtained from EDX

Concentration %	Elements	Wt.%	At%
0	Zn	81.68	60.98
	O	6.68	20.37
5	Zn	46.06	24.58
	Cu	4.74	2.60
	O	15.23	33.20
15	Zn	59.18	37.19
	Cu	10.20	6.60
	O	11.80	30.28
20	Zn	37.69	18.50
	Cu	12.32	5.74
	O	21.20	44.52

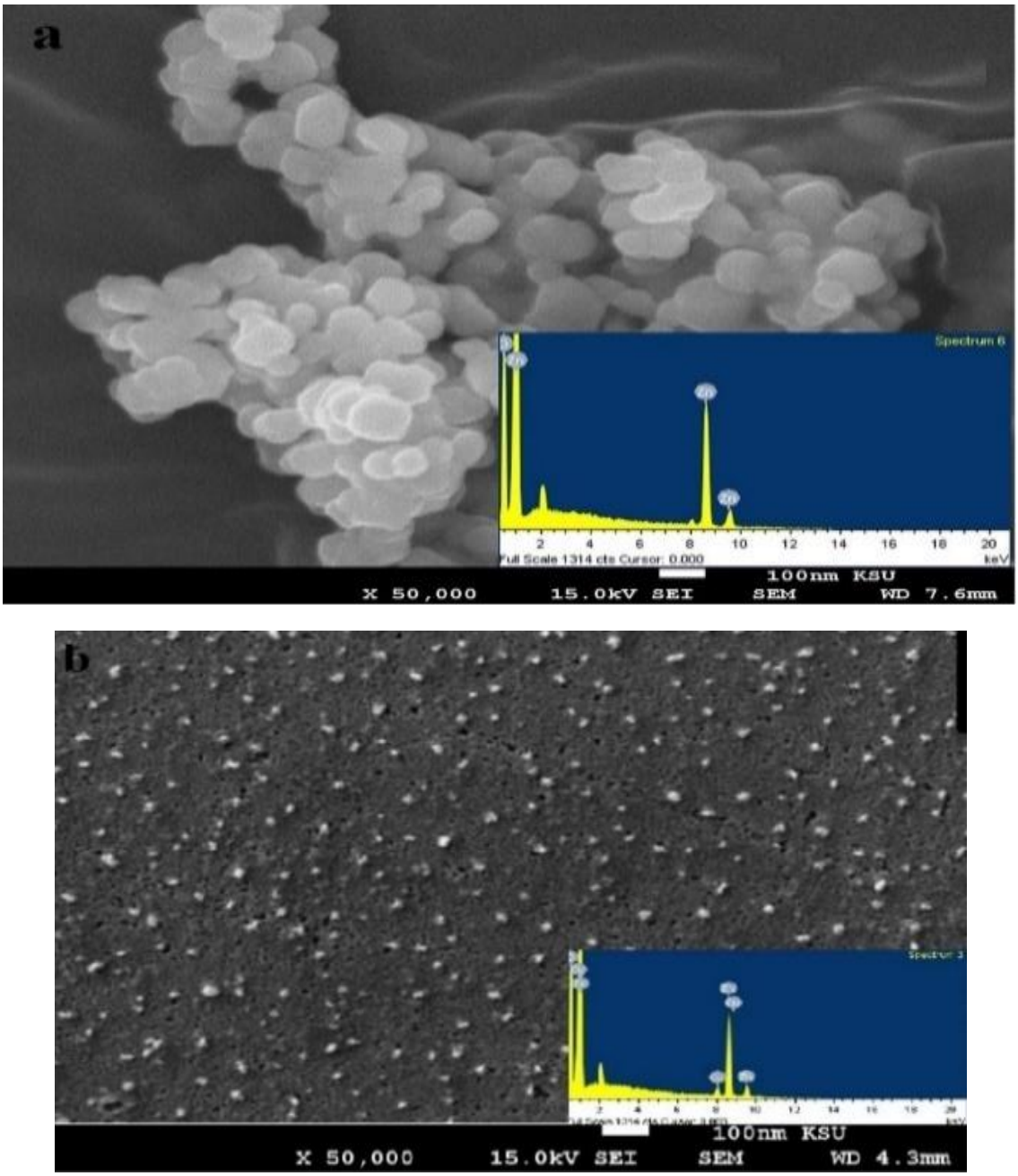

Fig. 1. SEM micrographs of ZnO films annealed at (a) 550^{0}c, (b) 20 wt. % Cu doped ZnO film

The annealing temperature (T_C) effect was observed on both intensities of XRD peaks and lattice parameters as shown in Fig. 2. Crystallite sizes of the deposited films have been calculated using (002) plane. The values of crystallite sizes are obtained 7.01 nm for ZnO and 3.21 nm, 2.75 nm, 4.82 nm, 3.86 nm and 2.41 nm for ZnO: Cu samples with Cu concentrations 5%, 10 %, 15%, 20% respectively. The grain size values and lattice parameters with different Cu concentrations are given in the following Table 2. Lattice constant slightly vary with doping concentration of Cu but no linear relation with Cu concentration. The shift in the lattice parameter is mainly due to the dopant occupying interstitial positions in the lattice. It is observed that the crystalline size in the doped films does not vary in any regular pattern with Cu dopant concentration, which is attributed to the lattice disorder produced in the films at higher dopant concentration due to difference in the ionic radii of Zn^{2+}amd Cu^{2+} ions and the combination of two different structures, hexagonal and cubic.

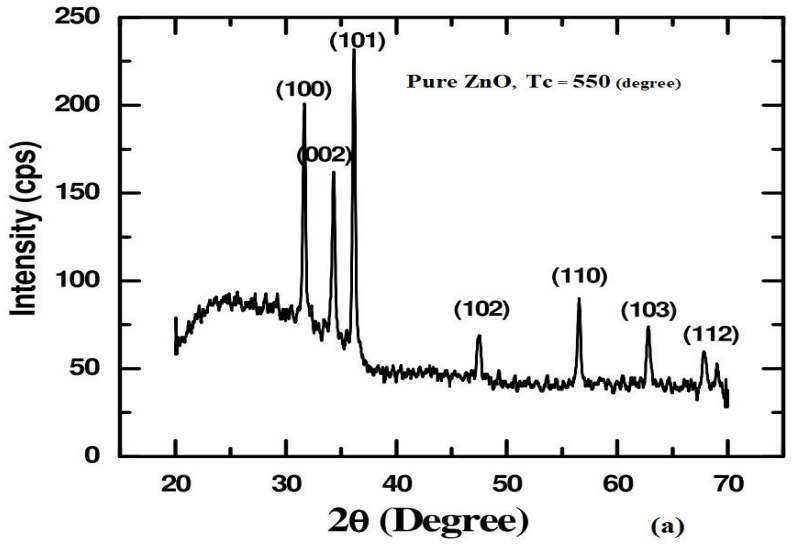
Intensity (cps)
2θ (Degree)
Pure ZnO, Tc = 550 (degree)
(100)
(002)
(101)
(102)
(110)
(103)
(112)
(a)

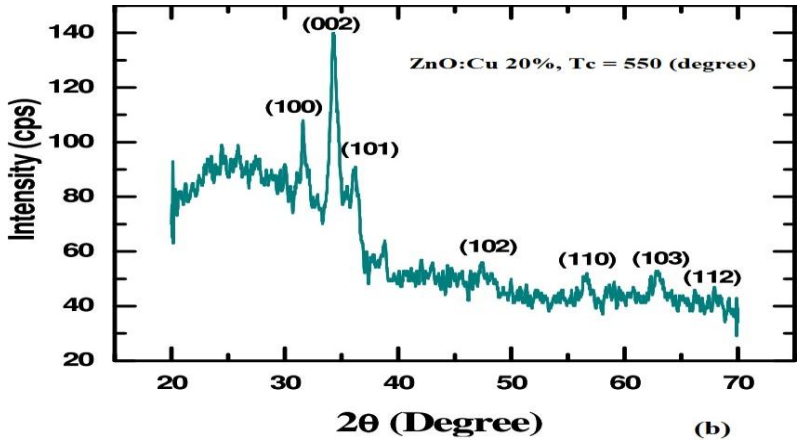
Intensity (cps)
2θ (Degree)
ZnO:Cu 20%, Tc = 550 (degree)
(002)
(100)
(101)
(102)
(110)
(103)
(112)
(b)

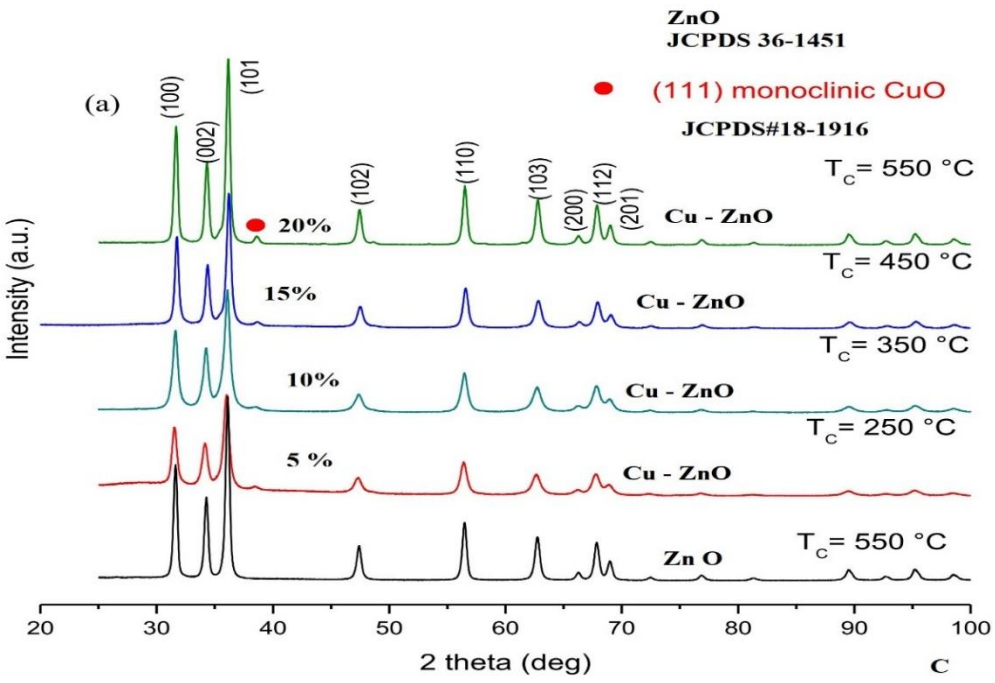
ZnO
JCPDS 36-1451
(111) monoclinic CuO
JCPDS#18-1916
(a)
(100)
(002)
(101)
(102)
(110)
(103)
(200)
(112)
(201)
20%
15%
10%
5 %
Cu - ZnO
Zn O
T_C= 550 °C
T_C= 450 °C
T_C= 350 °C
T_C= 250 °C
Intensity (a.u.)
2 theta (deg)
C

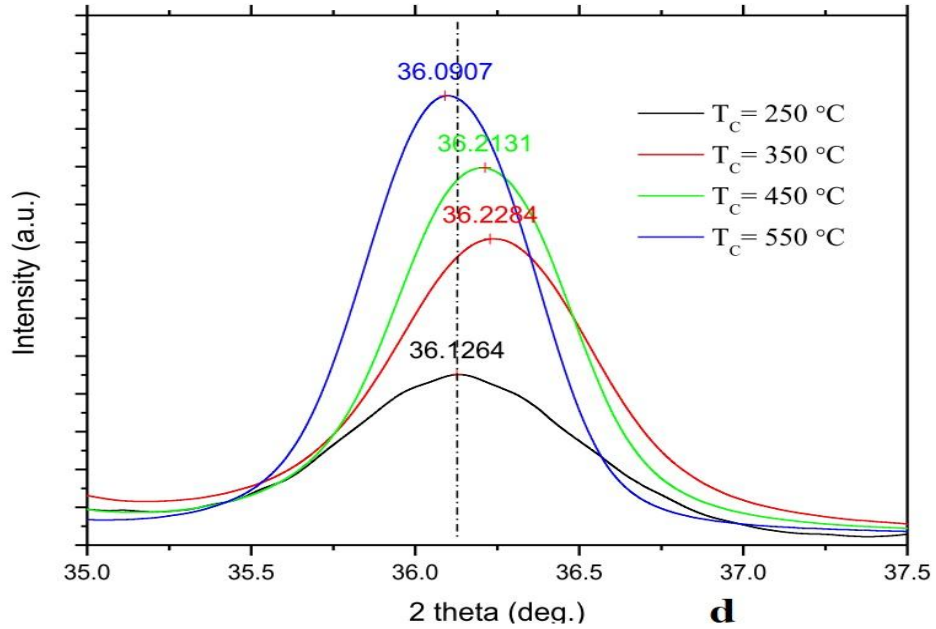

Fig. 2. XRD patterns for ZnO and Cu doped ZnO thin films for different Cu concentrations, (a) ZnO (b) ZnO: Cu 20%. (c) XRD patterns of ZnO different Cu concentration thin films with different temperature. (d) XRD principal peak shift due to the effects of the Cu doping and T_C

Table 2. Lattice parameters and grain size of undoped and Cu-doped ZnO thin *films*

Cu ZnO %	a (Å)	c (Å)	c/a ratio	Grain size (nm)
0	3.2604	5.2244	1.6024	7.01
5	3.2602	5.2277	1.6035	3.21
10	3.2678	5.2293	1.6002	2.75
15	3.2620	5.2210	1.6006	4.82
20	3.2674	5.2272	1.5998	3.86
JCPDS 36-1451	3.249	5.206	1.602	

3.3 Fourier Transform Infrared Studies (FTIR)

The chemical bonding and formation of wurtzite structure in ZnO and Cu-doped ZnO were confirmed by FTIR measurements at room temperature. The spectra are shown in Fig. 3. The broad absorption band at 3439.39, 1077.74, 3446.53 and 1075.74 cm^{-1} can be attributed to the normal polymeric O-H stretching vibration of H_2O, respectively in ZnO and Cu - ZnO lattices [33]. Other sharp peaks observed at 1621.45 and 1615.60 cm^{-1}can be attributed to H–O–H bending vibration, which in turn can be assigned to the small amount of H_2O in the ZnO and Cu – ZnO nanocrystals [34]. The absorption band observed between2300 and 2400 $cm^{-1}$are due to the existence of CO_2molecule in the air. The vibration band at446.31 cm^{-1}assigned to the stretching mode of ZnO, shifted to a lower frequency at 438.48 cm^{-1} for Cu - ZnO. Hence, it is supposed that Cu-ion can be successfully substituted into the crystal lattice of ZnO [35].

3.4 Surface Area Analysis (BET)

Fig. 5 shows the nitrogen adsorption-desorption isotherms and Barett Joyner–Halenda (BJH) pore size distribution for ZnO and Cu-doped annealed at 550^0C. All the isotherms obtained are Type IV and correspond to a capillary condensation, according to the classification of the International Union for Pure and Applied Chemistry (IUPAC). The hysteresis is Type H3, and is characteristic of the mesoporous material with slit-shape pores. Based on the results obtained from Fig. 4, the adsorption of N_2 on ZnO and Cu – ZnO catalysts, slightly increased from a low relative pressure of about 0.02 to 0.8 at higher T_C (450 and 550^0C) to 0.6 at lower T_C

(250 and 350^{0}C), and then followed by a sharp rise from 0.6 or 0.8 and above due to substantial interparticle porosity [36]. The highest and least volume of absorbed N_2 can be attributed to the catalysts annealed at T_C equal to 250^0 and 550^0 C, respectively. All the desorption branches are different from those of adsorption, indicating differences in their pore's texture [37]. Among all the catalysts, Cu -ZnO annealed at T_C = 250^0 C showed the highest volume of adsorption and widest desorption branch as shown in Fig. 4. The Barret–Joyner–Halenda (BJH) pore size distribution for all catalysts is shown in Fig. 4. All plots are located in the mesoporous range, which is in good agreement with the Type IV adsorption isotherm. The BJH pore size distribution of ZnO and Cu – ZnO annealed at T_C = 550^{0}C (Fig. 5) indicates different features of Cu – ZnO annealed at TC = 250, 350 and 450^{0}C, specifically from the average pore diameter centered at around 70 nm. This shows the result of the modification in pore texture. Based on the obtained results, it can be suggested that the annealing temperature has a clear effect on specific surface area and pore size distribution of the doped catalysts. On the other hand, for the same T_C = 550 ^{0}C, the obtained isotherms for ZnO and doped ZnO are very similar, showing almost the same specific surface area. This shows that the effect of doping is less important than the annealing temperature. By increasing the annealing temperature, a remarkable decrease in surface area of ZnO and Cu – ZnO can be observed. This phenomenon could be explained by clogging pores caused by the occurrence of possible aggregation when the annealing temperature increases. This may have the effect of clogging as observed in the diminution of both volume and average pore size.

3.5 Thermal Analysis of the Prepared Xerogel Catalysts

The thermal stability of the prepared ZnO and Cu – ZnO by the fast sol–gel method was studied by TGA and DTG as shown in Fig. 5a, b. For the ZnO, the weight loss of the xerogel occurred principally in two steps. In the first step, weight loss (8 %) was in the range of 80–178^{0}C, due to the dehydration of the absorbed surface water, as well as hydrate from the remaining zinc acetate and methanol solvent. In the second step, weight loss occurred in the range from 190 to 244^{0}c, which corresponds to 17 % due to the decomposition of tartaric acid. In the last step, weight loss ranged from 284 to 482 ^{0}C due to the conversion of zinc tartarate to zinc oxide and the percentage of weight loss was found to be 41.5 %. After 482 ^{0}C, no weight loss was observed and zinc oxide formed was further confirmed by XRD. On the other hand, for Cu – ZnO, a total weight loss of 7.9 % was observed in all four steps, and this is very low as compared with ZnO xerogel (64.5 %), indicating an increase in its stability due to the presence of Cu.

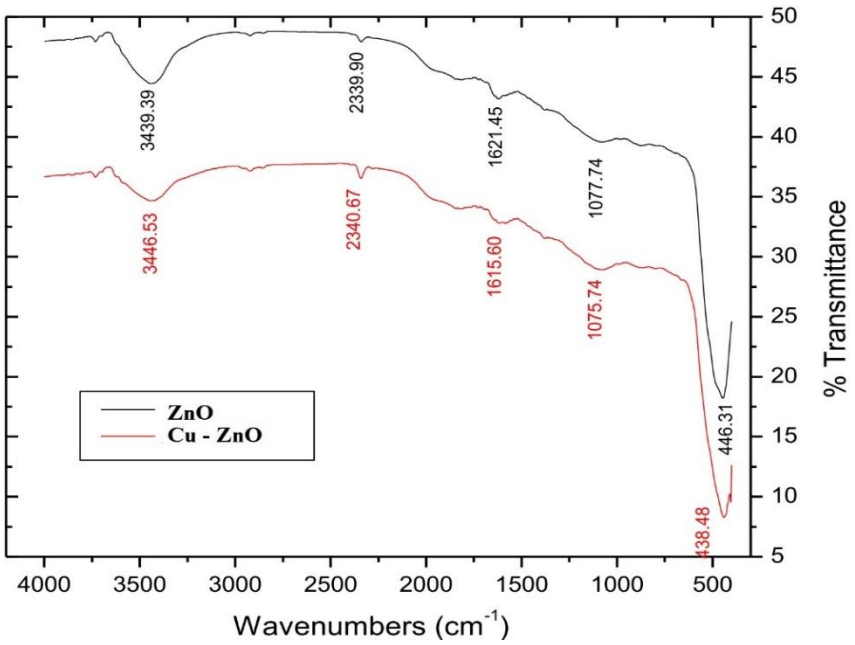

Fig. 3. FTIR spectra of ZnO and Cu-doped ZnO annealed at 550^{0}C

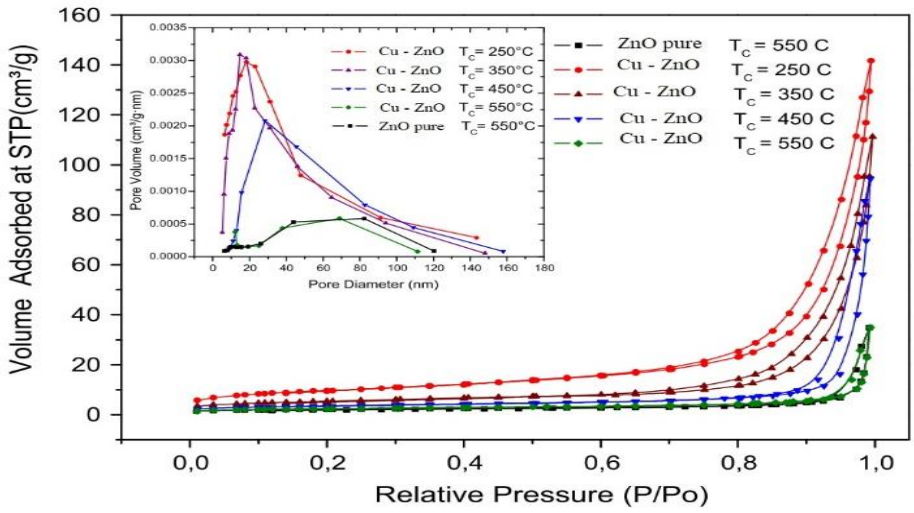

Fig. 4. N_2 adsorption-desorption isotherms and pore size distribution (inset) of ZnO and Cu-doped ZnO annealed at different temperature

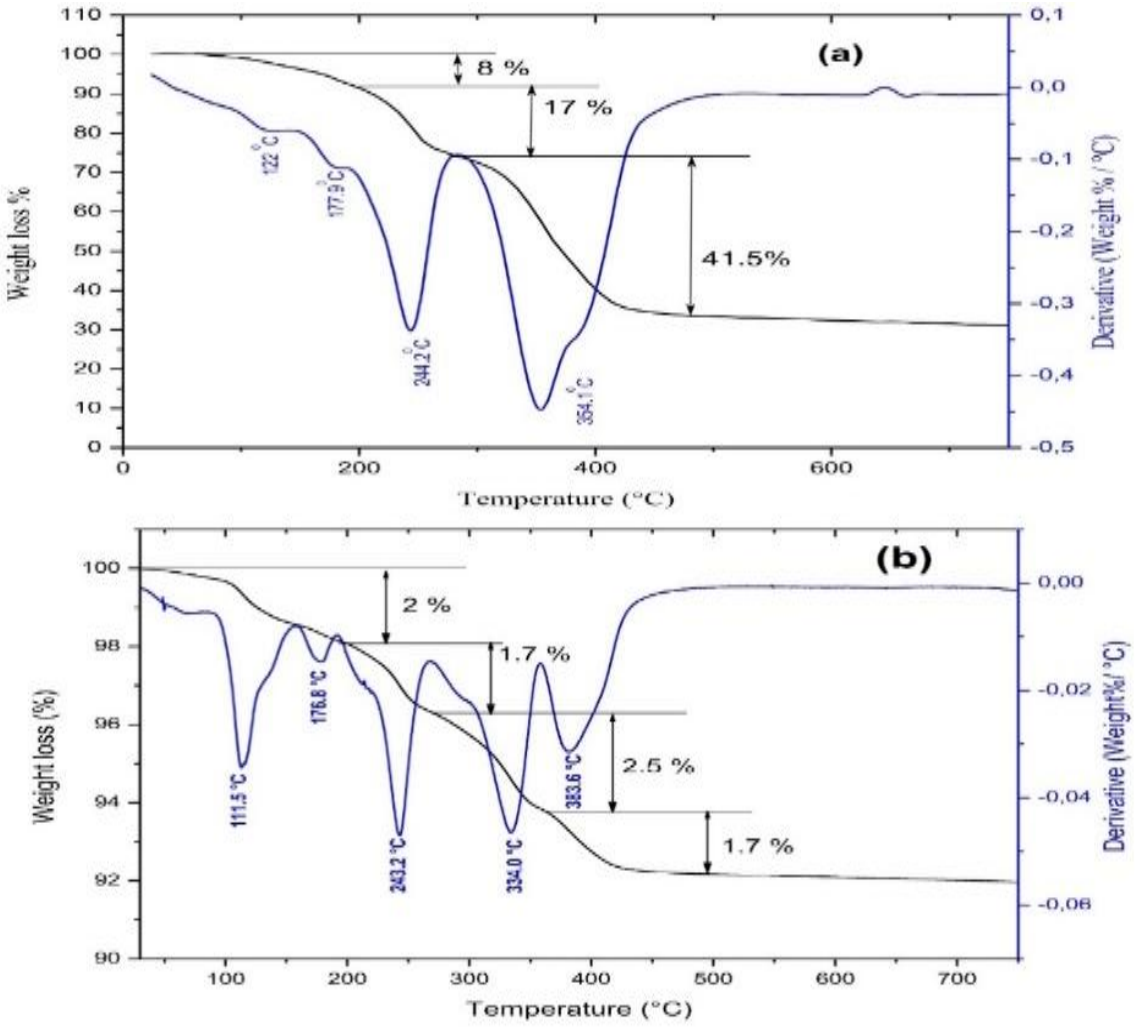

Fig. 5. TG-DTG analysis of (a) ZnO and (b) Cu – ZnO xerogel powders

3.6 Characterization of ZnO and Cu – ZnO by Photocatalytic Degradation of Malachite Green

The photocatalytic performances of ZnO and Cu-doped ZnO samples were investigated under UV light through the degradation of Malachite Green (MG), as a model organic pollutant. Fig. 5 shows the photodegradation activity of ZnO annealed at 550 ^{0}c and Cu – ZnO annealed at T_C of 250–550 ^{0}c photocatalysts. The results show that there is no degradation in the absence of the photocatalyst. On the other hand, the photocatalytic activity of ZnO was found to be very low: only 20 % of MG was degraded after 3h of irradiation. However, after doping ZnO with copper significantly increased its photocatalytic efficiency towards the degradation of MG. However, the efficiency of ZnO was significantly increased after doping with copper. As observed in Fig. 5, the kinetics were well fitted to pseudo first order then, the obtained values of the rate constant using Origin.8 software were plotted against the annealing temperature. It's known that the photocatalytic activity is related to the surface area of the photocatalyst. The present results were showed that the Cu-doping ZnO and the annealing temperature have played a crucial role on the enhancement of the photocatalytic efficiency by increasing the surface area. Nevertheless, this is not simply a question of specific surface area and adsorption, despite the fact that adsorption is a very important step in the photocatalytic process. Fig. 6 shows the adsorption in the dark, which depends to the nature of the catalyst. The most adsorbed quantity of the MG was found over the Cu-doped catalyst annealed at T_C = 250 ^{0}C. This result is in a good agreement with the obtained specific surface area value (35.10 m^2/g), but this catalyst was found to be less photoactive towards MG degradation, among other Cu-doped catalysts. Itis also important to note that the photocatalytic efficiency towards the degradation of MG with Cu – ZnO increased with increase in annealing temperature and formation of a CuO phase on the surface. This clearly demonstrates that photocatalytic activity depends on the annealing temperature rather than particles size and surface area. Similarly, it was shown that the photocatalytic activity of a catalyst is related to its microstructure, such as crystal plane, crystallinity, surface properties, BET specific surface area [38]. Many studies have shown that the difference in photocatalytic activity among all catalysts, not only related to the surface adsorption ability, but also to the type and concentration of oxygen defects on the surface and/or surface layers. Two major parameters can be affected by the annealing temperature: the increase in crystallinity and decrease of surface OH groups. Normally, since photocatalysis is a surface phenomenon, the decrease in surface OH groups may cause a loss in photocatalytic activity. However, the highest photoactivity in terms of MG degradation rate or kinetic constant was obtained from the catalyst annealed at the highest temperature (T_C = 550^{0}C) and with the lowest specific surface area (8.66 m^2/g). Therefore, an optimal quantity of hydroxyl groups on the catalyst surface in combination with a certain degree of crystallinity, and specific kinds of oxygen defects on the surface and /or surface layers are required to achieve optimal photoactivity [35]. In this study, the increase in photocatalytic activity of Cu - ZnO T_C = 550^{0}C may be attributed to the good crystallinity and oxygen defects as reported for ZnO [39]. However, the increasing crystallinity level with annealing temperature and the introduction of the native defects in the catalyst crystal in the form of neutral (VO), singly charged (VO+) or doubly charged (VO++) oxygen vacancies at higher annealing temperatures, may play a major role in the enhancement of its photocatalytic efficiency [40]. It is well known that these defects in the nanoparticles reduce the electron-hole recombination; hence increase the quantum yield and thus, enhance the photocatalytic activity. Furthermore, a high concentration of oxygen vacancies on the catalyst surface at higher annealing temperature and CuO phase can also serve as trap for electrons from the conduction band [41].

3.6.1 Adsorption kinetics of MG dye

Kinetics adsorption were studied using 250 ml of MG solution with initial concentration of 300 mg/L and 750 mg of solid was added and stirred in the dark. A sample was withdrawn every 15 min, diluted, centrifuged and residual concentration measured by spectrophotometer [Labomed – UVS-2800] at a maximum wavelength of 618 nm. The quantity of MG adsorbed per gram of catalysts at time (min) is calculated using following equation [42]:

$$q_t = \frac{(C_0 - C_t)V}{m} \quad (4)$$

Where q_t is the quantity of adsorbed MG per gram of adsorbent (catalysts)at time t, C_0 is the initial MG concentration, Ct the concentration of MG at time t, V is the volume of the MG solution

(ml) and m is the mass of the solid used (mg). All the data was fitted using pseudo-first order nonlinear Lagergren model [43]:

$$q_t = q_e(1 - e^{-kt}) \quad (5)$$

This kinetics are shown in Fig. 7 for the ZnO and the Cu – ZnO photocatalysts annealed at different temperatures (T_C). As it can be seen all kinetics obey to the first order according to Lagergren model (Equation 5) experimental data are represented by scatter points and Lagergren simulation by continuous line. However, it can be deduced from Fig. 7, stirring the MG + catalyst suspensions must be maintained in the dark for at least60 min which represents the solid saturation time (t_{sat}) prior to the degradation reaction.

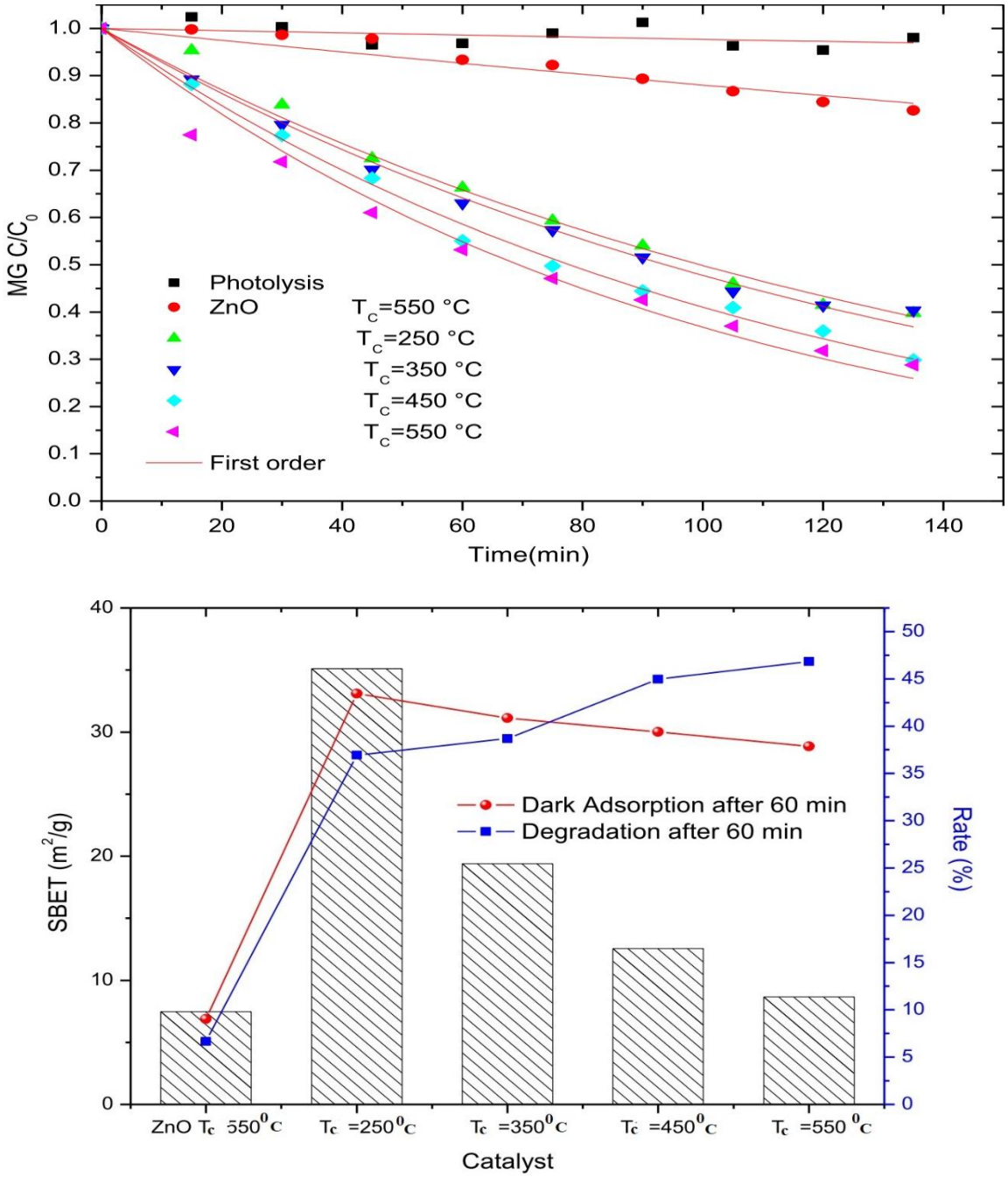

Fig. 6. Effect of mesoporous catalysts on dark adsorption after60 min, and degradation of (MG) and (SBET m^2/g)

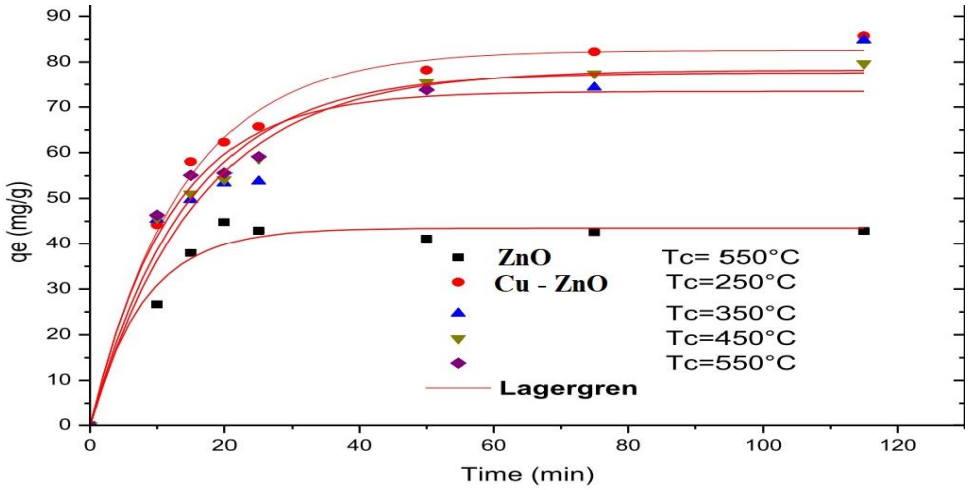

Fig. 7. MG Adsorption kinetics on catalysts annealed at different temperatures and Lagergren simulation

Fig. 8(a) and (b) show, the effects of annealing temperature on the apparent adsorption kinetic constants (k_{ads}) and equilibrium adsorbed amounts (q_e) deduced from the Fig. 7 by the Lagergren simulation. For the same annealing temperature (T_C = 550°C), doping ZnO with Cu decreases the rate of adsorption reaction Fig. 8 (a) but in contrast the equilibrium adsorbed amount (q_e) is approximately doubled (1.7 times higher; Fig. 8 (b) which can be explained by both: increasing of the specific surface area (1.15 times higher) and increasing site numbers created by the presence of copper (1.4 times higher). On the other hand, the adsorption rate seems to depend on both annealing temperature and specific surface area. In deed the normalized adsorption rate constant increases gradually with the increase of T_C.

3.6.2 Photocatalytic degradation of MG mechanism

When mixtures of MG aqueous solution and a suspension of photocatalyst were irradiated with VU light, the green solution of MG markedly changed, as a result of the decomposition of the free radicals formed in the solution. The photocatalytic activity mechanism of Cu-ZnO can be understood as follows: The Cu doped ZnO resulted in the creation of intermediate energy levels, which cause a delay in the recombination of charge carriers, thereby enhancing the photocatalytic activity. Moreover, it can be noticed that the delay in the recombination of charge carriers increases whenever the crystallinity of Cu –ZnO photocatalyst is improved by the annealing temperature rise. In the mechanism of photodegradation of MG in the presence of Cu –ZnO photocatalyst. The excitation of photocatalyst by UV light results to the formation of electron e^-_{CB} in both Cu/ZnO and CuO conduction bands. The direct bandgap of ZnO and ZnO/CuO is estimated by Tauc's formula, $(\alpha h\upsilon)^n = B\left(h\upsilon - E_g\right)$, where ***B*** is a constant related to the material, ***hυ*** is the photon energy in eV, ***h*** is Planck's constant, ***Eg*** is the optical bandgap in eV, n is an exponent that can take a value of either 2 for a direct transition or 1/2 for an indirect transition, and ***α*** is the absorption coefficient (in cm^{-1}) [44]. The electrons $\boldsymbol{e^-_{CB,CuO}}$ are transferred to the Cu/ZnO conduction band and then convert dissolved oxygen to super oxide radical. $\mathbf{O_2^-}$. While the holes $\mathbf{h^+_{VB,ZnO}}$ and $\mathbf{h^+_{VB,CuO}}$ from the CuO valence band level react with water to form the strongest oxidizing agent, hydroxide free radical .OH. Both active species can decompose MG completely [45,46]. The mechanism is schematically depicted in Fig. 9 and Scheme 1.

Fig. 10 shows the effects of annealing temperature on the main properties of, prepared, catalysts: Several correlations can be observed as for example the decrease in the specific surface area due to a sintering phenomenon linked to the increase in temperature, which increases the size of the crystallites by aggregation and confirms the effect on the surface. However, it is important to note that the degradation of MG increases with the annealing temperature despite the drop in specific surface proving that the photocatalysis is not, mainly, due to the adsorptive capacity of the catalyst.

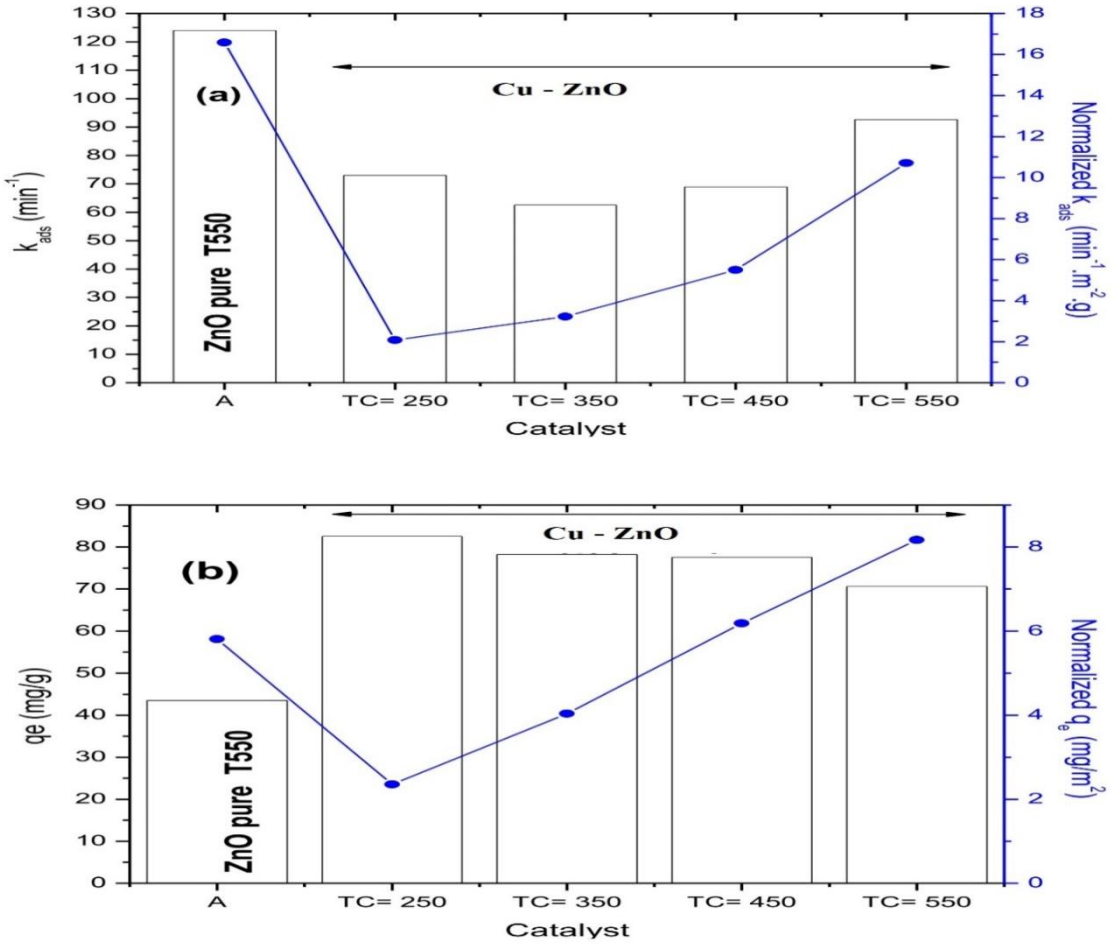

Fig. 8. Effect of annealing temperature (a) on the MG adsorption kinetic constant and (b) on the equilibrium MG adsorbed amount

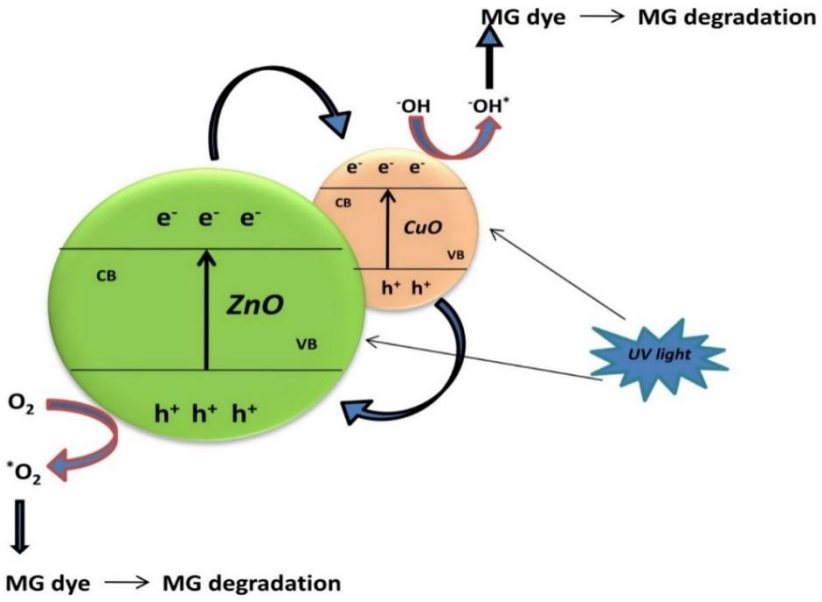

Fig. 9. Photocatalyst mechanism leading to the photocatalytic degradation of MG

CuO	+	hν	→	$e^-_{CB,CuO}$	+	$h^+_{VB,CuO}$		(1)
Cu/ZnO	+	hν	→	$e^-_{CB,ZnO}$	+	$h^+_{VB,ZnO}$		(2)
$e^-_{CB,CuO}$	→	Cu/ZnO	→	$e^-_{CB,ZnO}$				(3)
$h^+_{VB,ZnO}$	→	CuO	→	$h^+_{VB,CuO}$				(4)
$e^-_{CB,ZnO}$	+	O_2	→	$\mathbf{^\circ O_2^-}$				(5)
$h^+_{VB,CuO}$	+	H_2O	→	**°OH**	+	H^+		(6)
$^\circ O_2^-$	+	H^+	→	$^\circ O_2H$				(7)
$^\circ O_2H$	+ $^\circ O_2^-$	+	H^+	→	H_2O_2	+	O_2	(8)
$e^-_{CB,ZnO}$	+	H_2O_2	→	**°OH**	+	OH^-		(9)
$^\circ O_2^-$	+	MG	→	Degradation Products				(10)
°OH	+	MG	→	Degradation Products				(11)

Scheme 1. Proposed MG degradation mechanism

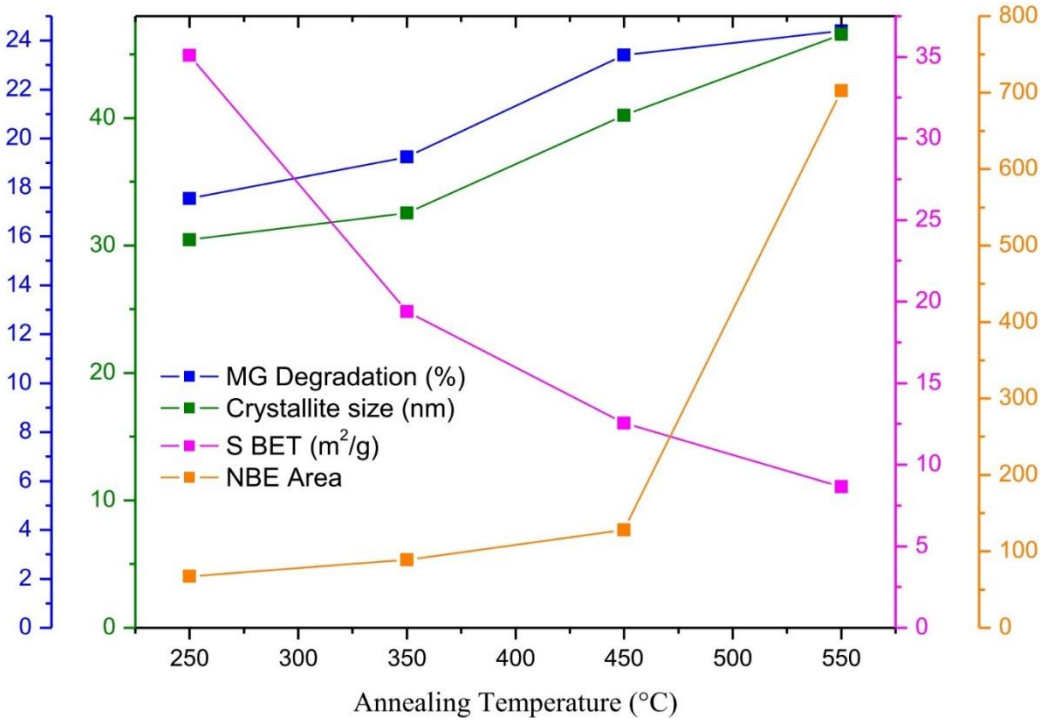

Fig. 10. Dependences and correlation between NBE area, SBET and crystallite size and MG degradation on the annealing T_c

3.7 Optical Properties

The optical transmission spectra of all samples in the visible region is a very important factor in many applications. So, measured at room temperature are illustrated in Fig. 11. All transmission spectra indicate sharp absorption edge. Moreover, as Cu composition increases,

the transmission spectra exhibit the obvious blue shift of absorption edge of an optical band gap of the film and highly transparent within a visible region with increasing Cu composition. From the graph it is seen that the values of transmittance are high in the visible and IR region and it is minimum in the UV region. These spectra show high transmittance near about 75 -85% in the wavelength range from 400-1100 nm. For direct transition the observed optical band gap depends on the doping concentration and varies from 3.21 eV to 3.05 eV which is shown in Table 3. Similar result was also reported by Lee, H. J. et al [47]. The variation of direct band gap energies with different doping concentration of Cu is shown in Fig. 9 with wavelength range 300 nm -1100 nm. Table 3 refer to variation of band gap of Cu ZnO thin films with different doping concentration of Cu. The optical absorption spectra are shown in Fig. 12 with wavelength range 300 nm - 1100 nm. The figures show the variation of absorbance with the doping concentration of copper. From the figure it is seen that the optical absorption decreases with the doping concentration of copper of the Cu - ZnO thin films [48]. These spectra show high absorbance in the wavelength range from 300-400 nm. The optical band gap can be determined by analyzing the transmission data using the classical relation [49],

$$\alpha h\nu = A\,(h\nu - E_g)^n \qquad (6)$$

where, ***A*** is a constant, "***h v***" is the photon energy and "E_g" is the optical band gap of the semiconductor and "***n***" is index related to the density of states for the energy band and is determined by the nature of optical transition involved in the absorption process. It is observed that small amount of Cu present in the films greatly affects the optical band gap of ZnO. The band gap decreases as the Cu concentration increases. Researcher think that this shift of the band gap with the Cu incorporation interpreted as mainly due to the sp-d exchange interactions between the band electrons and localized d electrons of the Cu^{+2} ions substituting Zn ions. The s-p and p-d exchange interactions give rise to a negative and a positive correction to conduction and valance band edges, leading to narrowing the band gap [50]. The nature of this variation in the band gap energy may be useful to design a suitable window material in fabrication of solar cells, means this thin-film technologies, that are still in an early stage of ongoing research or with limited commercial availability, are often classified as emerging or third generation photovoltaic cells and include, organic, dye-sensitized, and polymer solar cells, as well as quantum dot, copper zinc, nanocrystal, micromorph and perovskite solar cells. The variation of direct band gap energies with different doping concentration of Cu is shown in Fig. 13 (f).

3.8 Photoluminescence

The technique of photoluminescence excitation has become a standard one for obtaining information on the nanostructures. The photoluminescence excitation technique involves scanning the frequency of the excitation signal and recording the emission within a very narrow spectral range. In this study, the photoluminescence (PL) spectra of ZnO nanoparticles were estimated, to explore the effect of Cu-doping and annealing temperature on its optical properties. Fig. 14 shows the emission spectrum of ZnO and Cu - ZnO catalysts, using an excitation wavelength of 325 nm at room temperature. The photoluminescence (PL) emission was observed for all the samples (T_C = 250–550^{0}C) covering the range: from a short wavelength of 350 nm to a long wavelength of 550 nm. As the annealing temperature increased at 550^{0}c, all UV and visible luminescence also increased. The increase in UV emission may be ascribed to the improvement in observed crystalline quality due to annealing. The enhancement in blue emissions intensities is likely due to the strong exchange interactions between Zn and the second phase formed by Cu, after annealing of the sample. The first one, which originates from the recombination of free exciton [51], is clearly observed for ZnO at 379 nm. Thus, Cu -ZnO was annealed at the highest temperature T_C = 550 ^{0}C at 385 nm, and this may be attributed to exciton-related near-band edge emission (NBE). The second peak was observed according to the annealing temperature T_C at 417, 421, 428.5 and 430 nm, which corresponds to the blue emission [52]. As can be seen, the second peak seems to be observed only for Cu – ZnO catalysts, while the intensity of both peaks depends strongly on the annealing temperature. As the annealing temperature increases, the ultraviolet emission peak of the ZnO and Cu – ZnO catalysts, gradually, increases especially for T_C = 550°C. This increase was also observed for the blue emission peak for all annealing temperatures. For further understanding of the PL analysis, Fig. 15. (a)-(e) shows that all PL spectra are well fitted with a Gaussian function (the lowest

correlation coefficient is 99.4%). For ZnO the de-convoluted PL spectrum (Fig. 15. (a)) shows three peaks: two UV emission peaks of approximately the same intensity at 373 and 389 nm corresponding to the near-band emission of ZnO [53] and a violet emission peak at 410 nm with lower intensity. The effect of Cu doping can be seen at the same T_C = 550°C. By comparison of Fig. 15(a) and (b), it was observed that there is a red-shift of approximately 5 nm in the Cu-doped sample, which may correspond to a reduction in ZnO band gap due to Cu doping and the substitution of Cu ions into the Zn sites in the lattice as reported in the XRD study. Xu et al. [54] and Udayabhaskar et al. [55], reported similar results on Cu-doped ZnO, Ni-doped ZnO and Ca-doped ZnO materials, respectively. It was noticed that the violet peak at 410 in the ZnO completely disappeared this may be attributed to the defects and/or lattice imperfections of the ZnO sample, which can be removed by low-temperature thermal annealing. However, it seems that the peak was replaced by the two blue emission peaks in the Cu – ZnO mesoporous catalysts. The observation of visible emissions may be related to intrinsic defects in ZnO and their enhancement in the presence of Cu ions induced a poorer crystallinity and greater level of structural defects, which can be attributed to the more intrinsic defects introduced by Cu ion incorporation into the ZnO lattice. This result is in line with the above XRD findings. Xu et al. [54] related similar results to Raman observations regarding the defects gradually generated with the Cu doping ratio. The effect of annealing temperature T_C and its comparison is shown in Table 4 and Fig. 15 (a-e). As the annealing temperature increased from 250 to 550°C, all UV and visible luminescence increased. The increase in UV emission may be ascribed to the improvement in observed crystalline quality due to annealing. The enhancement in blue emissions intensities is likely due to the strong exchange interactions between Zn and the secondary phase formed by Cu, after annealing of the sample. Certainly, thermal annealing can provide more energy for the substitution of Zn atom sites by Cu atoms into the lattice of ZnO.

3.9 Electrical Properties

Resistivity of the prepared ZnO and Cu doped ZnO thin films have been measured by van-der Pauw method [56]. The resistivity measurement has been performed over a range from room temperature to 440 K. During the measurement, the temperature increased slowly as a result the whole film is heated with uniform temperature. The variation of resistivity with temperature for films and resistivity gradually decreases with the increase of temperature, which indicates the semiconducting nature of the materials is shown in Fig. 16. The electrical resistivity of ZnO was increased by doping Cu indicating the acceptor like behavior of the Cu dopant. The four coordinated Zn, Cu and Cu cations have ionic radii of 0.06, 0.06 and 0.057 nm respectively, with stable electronic configuration, Zn^{2+} ($3d^{10}$), Cu^{2+} ($3d^9$) and Cu^{+}($3d^{10}$). Diffusion at high firing temperature may lead defect reactions in which Cu^{2+} cations substitute Zn^{2+} cations in the wurtzite unit cell of ZnO. The stability of the coulomb forces of the interactions between the acceptor defect ($Cu^{1+}Zn$) and intrinsic ZnO donors may occur by capture of an electron from the lattice.

The variations of electrical conductivity with temperature for Cu ZnO thin films are shown in Fig. 17. From the figure it is seen that the conductivity increases with the increase of temperature. This type of variation indicates the semiconducting behavior of the films. The conductivity decreases with the increasing of Cu concentration [47]. Incorporation of Cu into ZnO reduces its conductivity as Cu introduces deep acceptor level and it traps electrons from the conduction band.

Table 3. Band gap of Cu ZnO thin films with different doping concentration of Cu

Sample	Concentration of Cu (%)	Direct band gap E_g in eV
Cu ZnO	0	3.21
	5	3.20
	10	3.19
	15	3.17
	20	3.16
	25	3.05

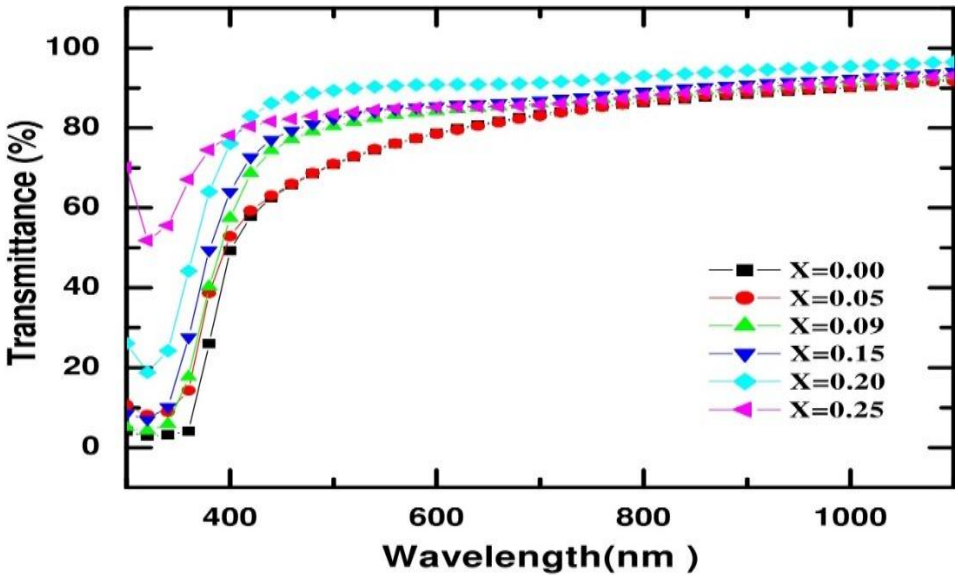

Fig. 11. Variation of optical transmittance with wavelength of Cu ZnO thin films for different concentration

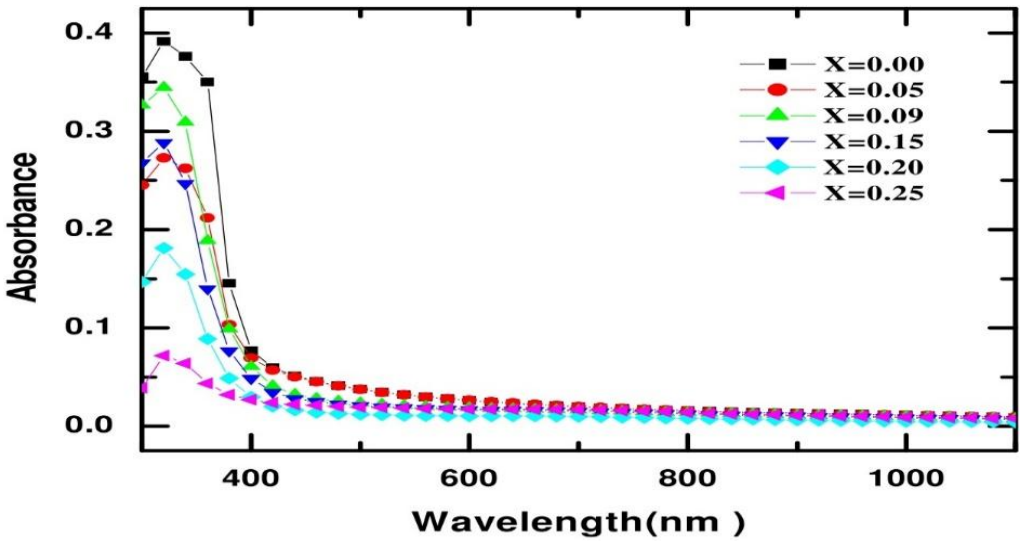

Fig. 12. Variation of optical absorption with wavelength of Cu ZnO thin films for different concentration

Table 4. Photoluminescence Emission Values of pure and Cu-doped ZnO deduced from de-convolution by Gaussian function of PL spectra

Catalysts	Near band edge, NEB (nm)	NEB intensity (a.u)	Blue emission (nm)
ZnO, T_c = 550°C	373- 389	32.40- 31.41	410(violet)
Cu – ZnO, T_c = 550°C	378	27.87	423. 45
T_c = 450°C	379	4.89	429. 46
T_c = 350°C	379	3.44	429. 46
T_c = 250°C	378	3.13	419. 45

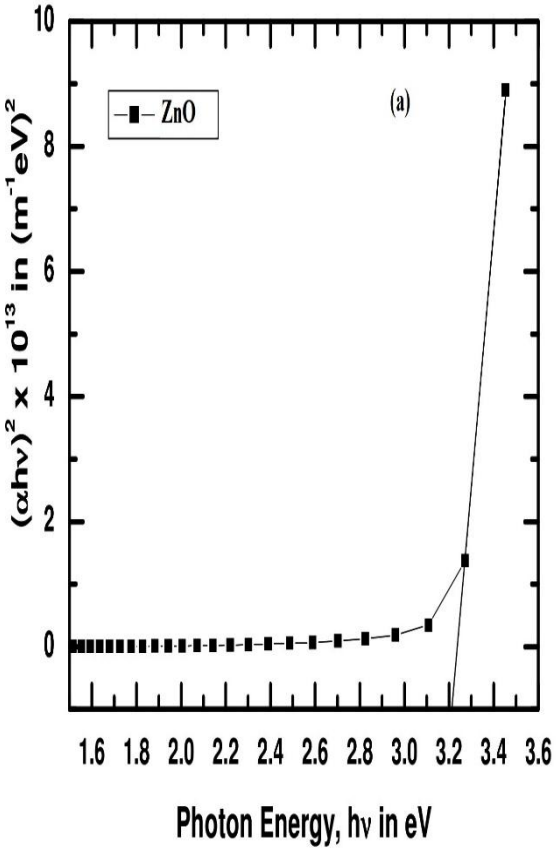
ZnO
(a)
$(\alpha h\nu)^2 \times 10^{13}$ in $(m^{-1}eV)^2$
Photon Energy, hν in eV

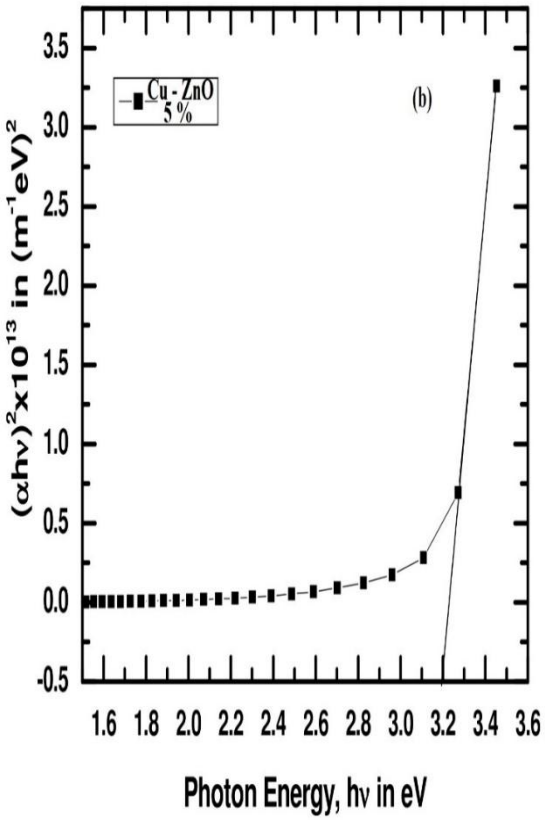
Cu - ZnO 5 %
(b)
$(\alpha h\nu)^2 \times 10^{13}$ in $(m^{-1}eV)^2$
Photon Energy, hν in eV

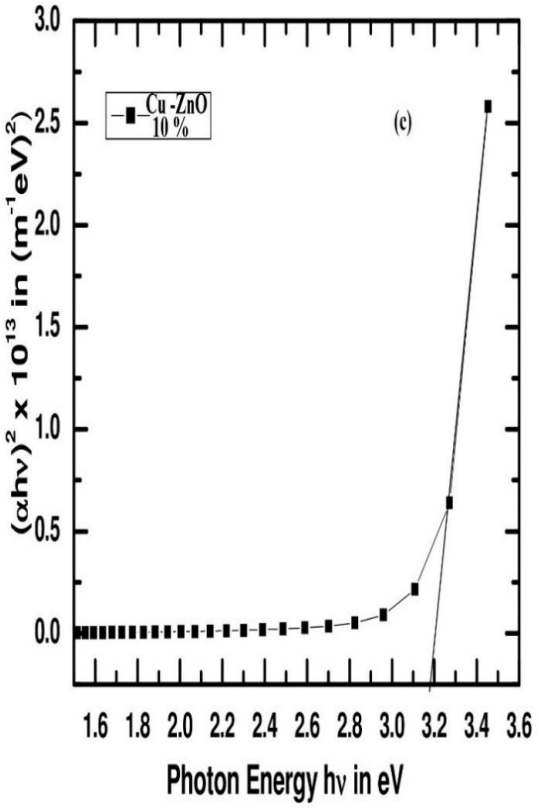
Cu -ZnO 10 %
(c)
$(\alpha h\nu)^2 \times 10^{13}$ in $(m^{-1}eV)^2$
Photon Energy hν in eV

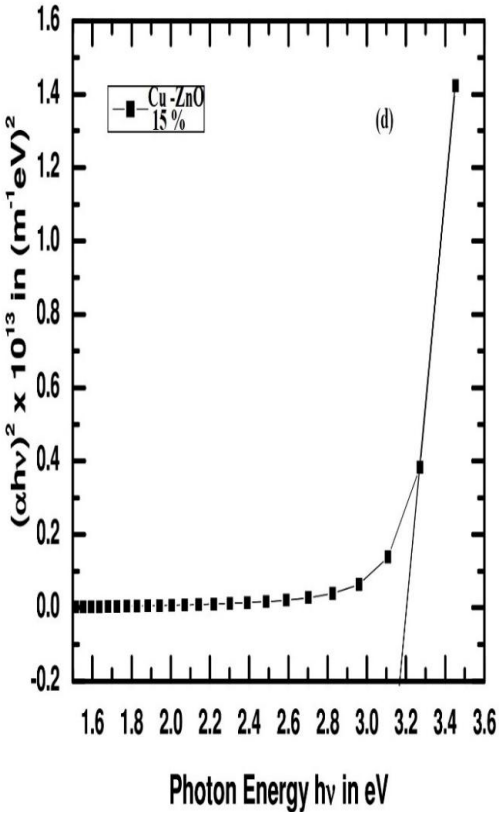
Cu -ZnO 15 %
(d)
$(\alpha h\nu)^2 \times 10^{13}$ in $(m^{-1}eV)^2$
Photon Energy hν in eV

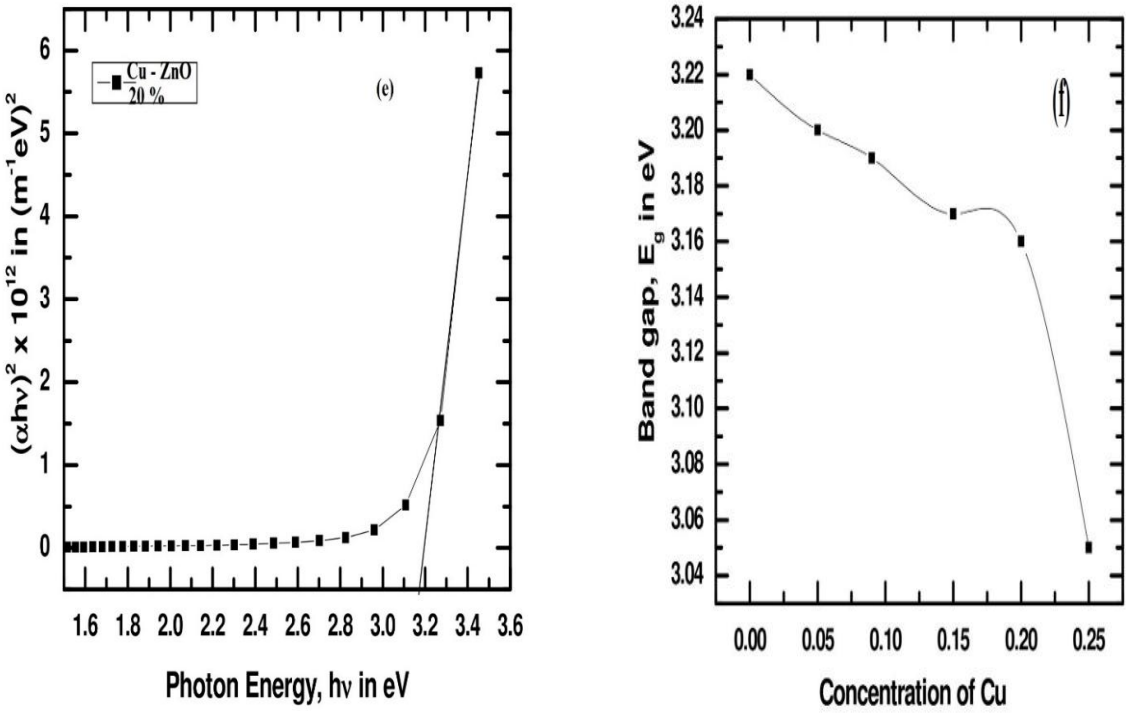

Fig. 13. Variation of $(\alpha h\ \nu)^2$ with photon energy for(a) ZnO. (b) 5% (c), 10%, (d), 15% and (e) 20% Cu doped ZnO thin film. (f) Band gap energies with concentration of Cu for Cu ZnO thin films

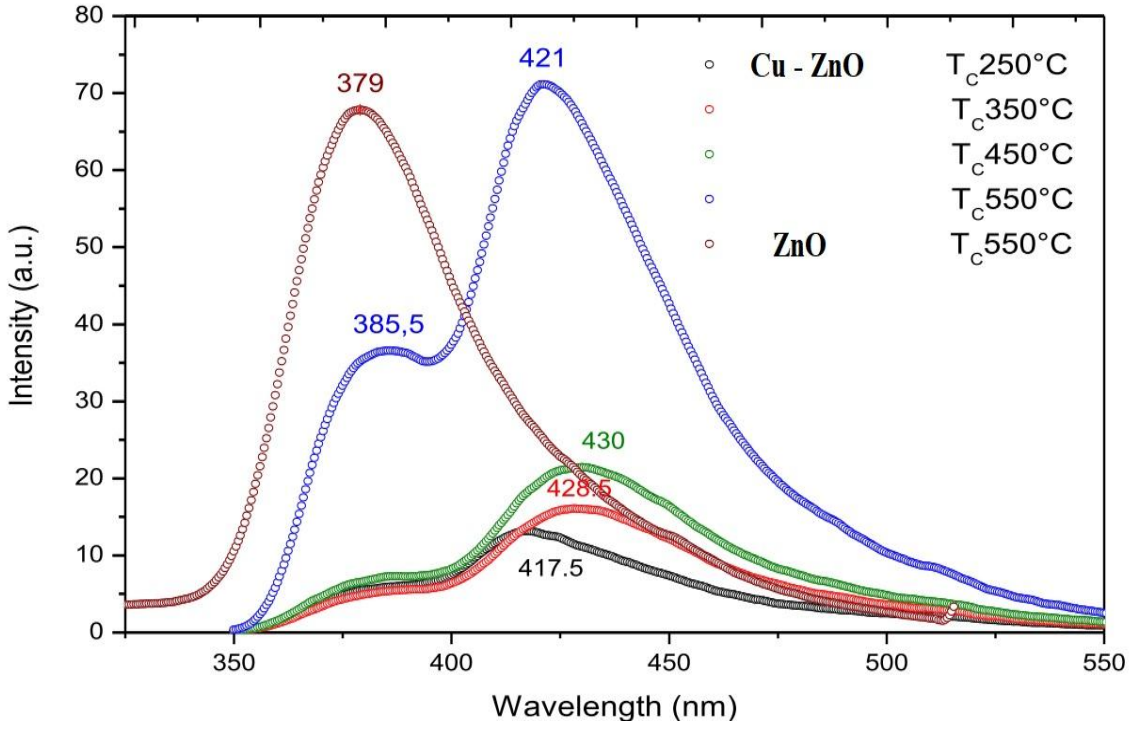

Fig. 14. PL Spectra of the ZnO annealed at 550°C and Cu-ZnO annealed at different temperatures at excitation wavelength 325 nm°C

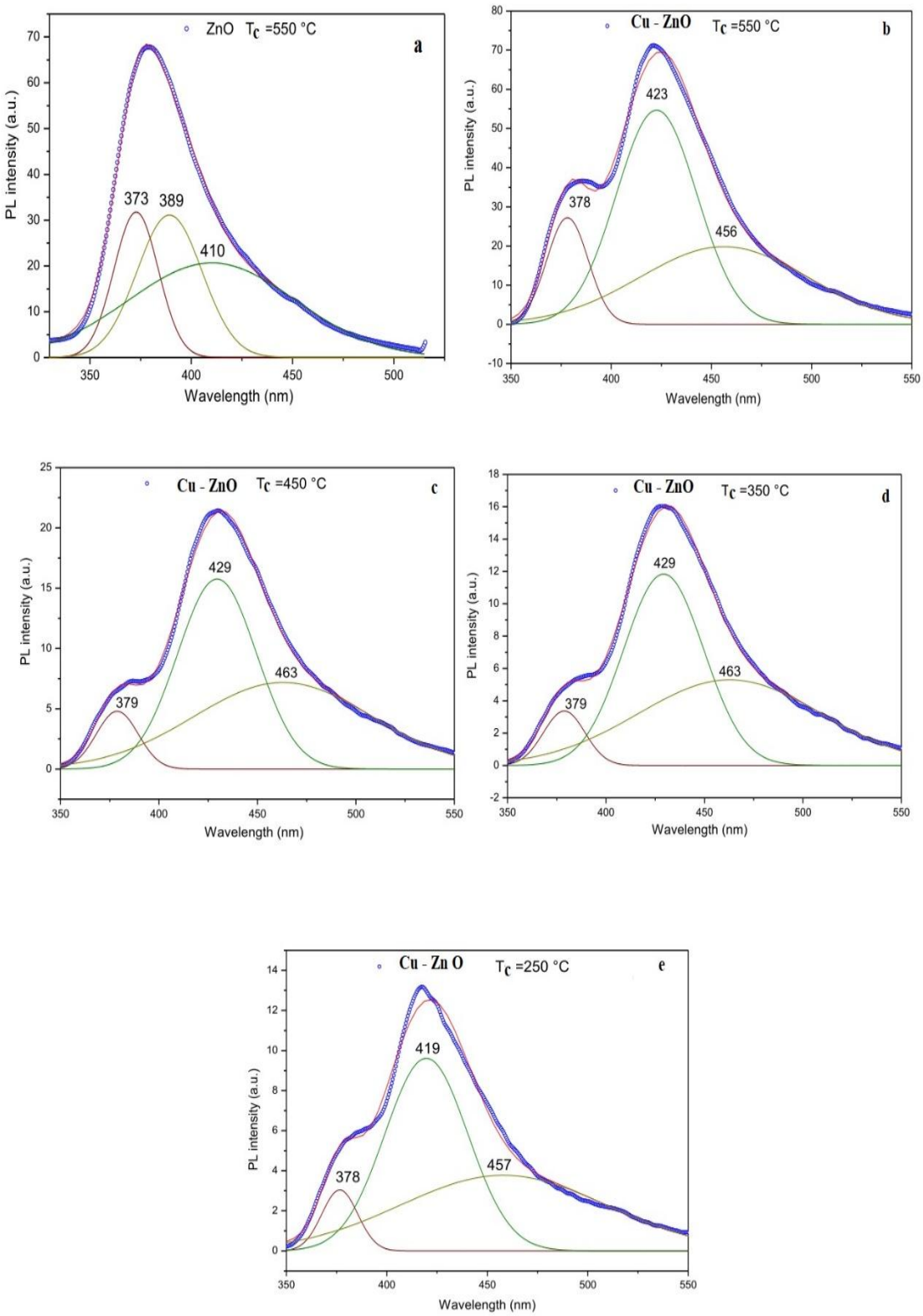

Fig. 15. PL emissions spectra of ZnO T_C = 550^{0}C, (b) Cu – ZnO T_C = 250^{0}C, (c) T_C = 350^{0}C, (d) T_C = 450^{0}C and (e) T_C = 550^{0}C NPs using the excitation wavelength at 325 nm

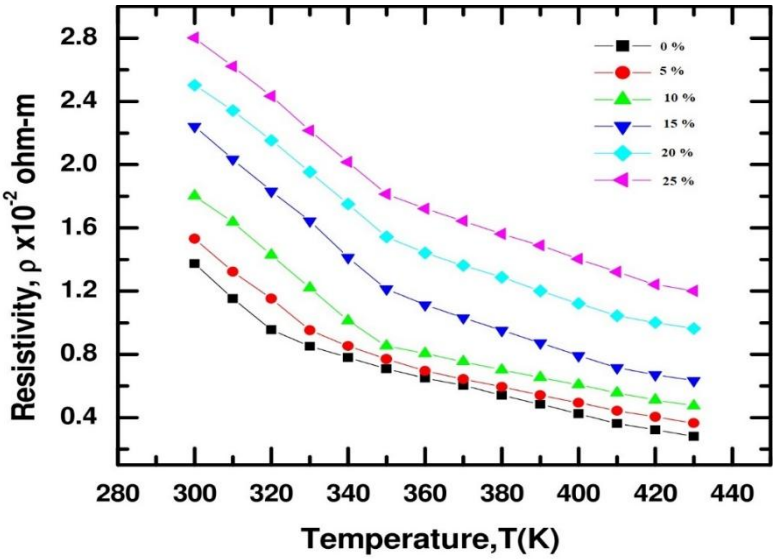

Fig. 16. Variation of electrical resistivity with temperature for Cu ZnO thin films

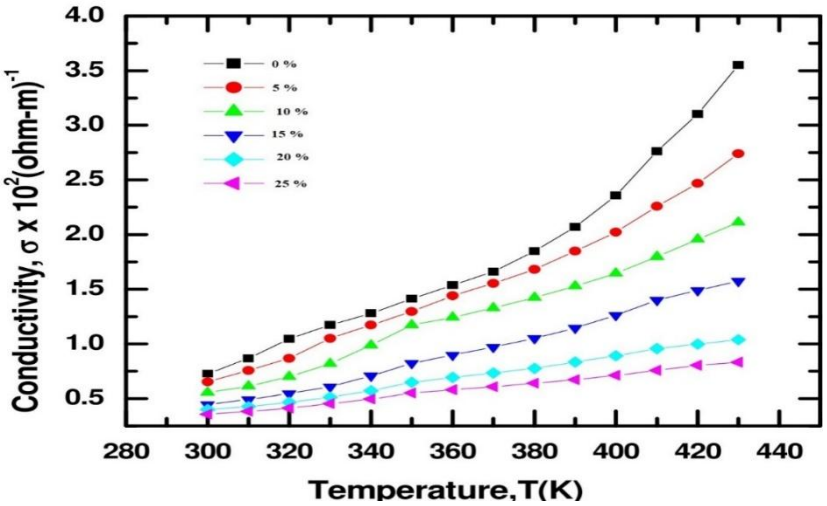

Fig. 17. Variation of electrical conductivity with temperature for Cu ZnO thin films

4. CONCLUSIONS

In the present work, Zinc oxide and Cu-doped ZnO thin films were synthesized by a sol–gel method in the presence of tartaric acid. The obtained powders were annealed at different temperatures. XRD studies confirmed the dominant presence of hexagonal wurtzite ZnO with the formation of monoclinic CuO phase on the surface of ZnO. Films of different doping concentration of Cu were deposited on glass substrate. it was shown that specific surface area decreases with annealing temperature due to the occurrence of the aggregation phenomenon. The photocatalytic ability showed that the catalyst activity was influenced by both different doping concentration of Cu loading on ZnO and annealing temperature. The Cu – ZnO catalyst annealed at 550 ^{0}C exhibited the highest photocatalytic activity due to the interlacing of several factors such as the efficient charge separation as proven by the PL spectra, the enhancement of crystallinity and the introduction of the native defects in the catalyst crystal in the form of neutral (VO), singly charged (VO^{+}) or doubly charged (VO^{++}) oxygen vacancies. Moreover, the CuO phase on the surface resulted in delayed recombination charge and increased the photocatalytic activity of catalysts at a higher temperature. Various optical constants such as absorbance, transmittance of the films have been studied for the as-deposited

films are recorded in the wavelength ranges from 300 to 1100 nm. The values of transmittance are high in the visible and IR region and it is minimum in the UV region. Absorbance decreases with higher percentage of Cu concentration. The band gap of the films varied 3.21 to 3.05 eV. The increase in the Cu incorporation in the film results in the overall decrease in the refractive index. The electrical resistivity measurements were made on number of films from the room temperature up to 430K. The figure shows that the resistivity gradually decreases with the increase of temperature, which indicates the semiconducting nature of the materials. Resistivity also increases with the increasing doping concentration. The conductivity decreases with the increasing of Cu concentration. Incorporation of Cu into ZnO reduces its conductivity as Cu introduces deep acceptor level and it traps electrons from the conduction band.

COMPETING INTERESTS

The author declares that there are no personal, organizational or financial conflicts of interest.

REFERENCES

1. Kavitha T, Yuvaraj H. A facile approach to the synthesis of high-quality NiO nanorods: Electrochemical and antibacterial properties. J. Mater. Chem. 2011;21: 15686-15691.
   DOI: 10.1039/C1JM13278D
2. Wu CC, Shih WC. Development of a highly transparent, low-resistance lithium-doped nickel oxide triple-layer film deposited by magnetron sputtering. Chem. Commun. 2017;53:1634–1637.
   DOI: 10.1039/C6CC08738H
3. Karali T, Can N, Valberg L, Stepanov AL, Townsend PD, Buchal Ch., Ganeev RA, Ryasnyansky AI, Belik HG, Jessett ML, Ong C. Optical properties and luminescence of metallic nanoclusters in ZnO: Cu. Physica B: Condensed Matter. 2005;363:88-95.
   doi.org/10.1016/j.physb.2005.03.006
4. Vikas Sharma, Inderjeet Singh, Amreesh Chandra. Hollow nanostructures of metal oxides as next generation electrode materials for supercapacitors. Scientific Reports. 2018;8. Article number: 1307. doi.org/10.1038/s41598-018-19815-y
5. Khan Mamun Reza, Kurny ASW, Fahmida Gulshan. Parameters affecting the photocatalytic degradation of dyes using TiO_2: A review. Applied Water Science. 2017;7(4):1569–1578. Available:https://link.springer.com/article/10.1007/s13201-015-0367-y
6. El-Hilo M, Dakhel AA, Ali-Mohamed AY. Room temperature ferromagnetism in Nanocrystalline Ni-doped ZnO synthesized by co-precipitation. Journal of Magnetism and Magnetic Materials. 2009;321:2279–2283.
   doi.org/10.1016/j.jmmm.2009.01.040
7. Mamat MH, Sahdan MZ, Khusaimi Z, Zain Ahmed A, Abdullah S, Rusop M. Influence of doping concentrations on the aluminum doped zinc oxide thin films properties for ultraviolet photoconductive sensor applications. Optical Materials. 2010;32: 696–699.
   doi.org/10.1016/j.optmat.2009.12.005
8. Li JH, Liu YC, Shao CL, Zhang XT, Shen DZ, Lu YM, Zhang JY, Fan XW. Effects of thermal annealing on the structural and optical properties of Mg_x Zn_{1-x} O nanocrystals. J Colloid Interf Sci. 2005; 283:513-517.
   DOI: 10.1016/j.jcis.2004.09.011
9. Krunks M, Dedova T, Açik IO. Spray pyrolysis deposition of zinc oxide nanostructured layers. Thin Solid Films. 2006;515:1157-1160.
   doi.org/10.1016/j.tsf.2006.07.134
10. Ramakrishna Murthy M, Venkateshwar Rao E. Ion-beam modifications of the surface morphology and conductivity in some polymer thin films. Bulletin of Materials Science. 2002;25:403–406. doi.org/10.1007/BF02708018
11. Abdelrahman MM, Osman M, Hashhash A. Electrical properties of irradiated PVA film by using ion/electron beam. Progress of Theoretical and Experimental Physics; 2016.
    doi.org/10.1093/ptep/ptv178
12. Fekete ZA, Wilusz E, Karasz FE, Visy C. Ion beam irradiation of conjugated polymers for preparing new membrane materials-A theoretical study. Separation Purification Technology. 2007;57:440–443.
    doi.org/10.1016/j.seppur.2006.04.014
13. Makuuchi K, Cheng S. Radiation processing of polymer materials and its industrial applications. (Copyright © 2012 John Wiley & Sons, Inc.). Online
    ISBN: 9781118162798.
    doi.org/10.1002/9781118162798.fmatter

14. Sahbeni K, et al. Annealing temperature effect on the physical properties of titanium oxide thin films prepared by the sol-gel method. Journal of Physical Chemistry & Biophysics. 2017;7:257.
Available:https://www.omicsonline.org/open-access/annealing-temperature-effect-on-the-physical-properties-of-titaniumoxide-thin-films-prepared-by-the-solgel-method-2161-0398-1000257.pdf
15. Abdolahzadeh Ziabari A, Ghodsi FE. Optical and Structural Studies of Sol-Gel Deposited Nanostructured CdO Thin Films: annealing effect. ACTA Physica Polonica A. 2011; 120.
Available:http://przyrbwn.icm.edu.pl/APP/PDF/120/a120z3p31.pdf
16. Agawane GL, Shin SW, Vanalaka SA, Jin Hyeok Kim. Synthesis of simple, low cost and benign sol–gel Cu_2ZnSnS_4 thin films: influence of different annealing atmospheres. J Mater Sci: Mater Electron. 2015;26:1900–1907.
DOI: 10.1007/s10854-014-2627-2
17. Kai Loong Foo, Uda Hashim, Kashif Muhammad, Chun Hong Voon. Sol–gel synthesized zinc oxide nanorods and their structural and optical investigation for optoelectronic application. Nanoscale Res Lett. 2014;9.
DOI: 10.1186/1556-276X-9-429
18. Özgür Ü, et al. A comprehensive review of ZnO materials and devices. J. Appl. Phys. 2005;98:041301-103.
Available:https://doi.org/10.1063/1.1992666
19. Vinod Kumar, et al. Rare earth doped zinc oxide nanophosphor powder: A future material for solid state lighting and solar cells. ACS Photonics. 2017;4(11):2613-2637.
Available:https://10.1021/acsphotonics.7b00777
20. Vinod Kumar, et al. Synthesis and characterization of aluminum–boron co-doped ZnO nanostructures. Material Research Bulletin. 2013;48:362.
Available:https://doi.org/10.1016/j.materresbull.2012.10.042
21. Rabia Qindeel, et al. Characterizations of multilayer ZnO thin films deposited by sol-gel spin coating technique. Results in Physics. 2017;7:651-655.
Available:https://doi.org/10.1016/j.rinp.2016.12.029
22. Amari R, et al. Structural, optical and luminescence properties of ZnO thin films prepared by sol-gel spin-coating method: Effect of precursor concentration. CHIN. PHYS. LETT. 2018;35(1):01680.
Available:https://10.1088/0256-307X/35/1/016801
23. Vinod Kumar, et al. Deep level defect correlated emission and Si diffusion in ZnO: $Tb3^+$ thin films prepared by pulsed laser deposition. J. Colloid and Interface Science. 2016;465:295.
Available:https://doi.org/10.1016/j.jcis.2015.12.007
24. Kaniz Naila Tonny, et al. Electrical, optical and structural properties of transparent conducting Al doped ZnO (AZO) deposited by sol-gel spin coating. AIP Advances. 2018;8:065307.
Available:https://doi.org/10.1063/1.5023020
25. Ziaul Raza Khan. Sol-gel derived Cds nanocrystalline thin films: Optical and photoconduction properties. Materials Science-Poland. 2018;36(2):235–241.
Available:https://doi.org/10.1515/msp-2018-0028
26. Sugi S, Usha Rajalakshmi, Shanthi J. Photocatalytic degradation Efficiency of $Cu_XZn_{1-X}O$ composite. Optik. 2017;131: 406-413.
doi.org/10.1016/j.ijleo.2016.11.030
27. Marco Laurenti, Valentina Cauda. Porous zinc oxide thin films: Synthesis approaches and applications. MDPI Coatings. 2018; 8(2):67.
Available:https://10.3390/coatings8020067
28. Kadam LD, Patil PS. Thickness-dependent properties of sprayed cobalt oxide thin films. Materials Chemistry and Physics. 2001;68:225–232.
Available:https://doi:10.1016/s0254-0584(00)00367-9
29. Hashim H, et al. Investigation of annealing temperature on copper oxide thin films using sol-gel spin coating technique. IOP Conference Series Materials Science and Engineering. 2018;340(1):012008.
Available:https://doi.org/10.1088/1757-899x/340/1/012008
30. Tolansky S. Multiple beam interferometry of surface and films. Oxford University Press, London; 1948.
31. Muniz FTL, Miranda MAR, Morilla dos Santos C, Sasaki JM. The Scherrer equation and the dynamical theory of X-ray diffraction. Acta Crystallographica Section A. 2016;A72:385-390.
doi.org/10.1107/S205327331600365X

32. Sharma RK, Patel S, Pargaien KC. Synthesis, characterization and properties of Mn-doped ZnO nanocrystals. Advances in Natural Sciences: Nanoscience and Nanotechnology. 2012;3(3):035005. Available:http://doi:10.1088/2043-6262/3/3/035005
33. Triloki, Garg P, Rai R, Singh BK. Structural characterization of "as-deposited" cesium iodide films studied by X-ray diffraction and transmission electron microscopy techniques. Cond-Mat. Mtrl-Sci. 2013; arXiv:1211.5540v3.
34. Alessio Becheri, Maximilian Dürr, Pierandrea Lo Nostro, Piero Baglioni. Synthesis and characterization of zinc oxide nanoparticles: Application to textiles as UV-absorbers. 2008;10:679–689. Available:https://link.springer.com/article/10.1007/s11051-007-9318-3
35. Muthukumaran S, Gopalakrishnan R. Structural, FTIR and photoluminescence studies of Cu doped ZnO nanopowders by co-precipitation method. Opt. Mater. 2012; 34:1946–1953. doi.org/10.1016/j.optmat.2012.06.004
36. Xiong G, Luo L, Li C, Yang X. Synthesis of mesoporous ZnO (m-ZnO) and catalytic performance of the Pd/m-ZnO catalyst for methanol steam reforming. Energy & Fuels. 2009;23(3):1342–1346. Available:http://doi:10.1021/ef8008376
37. Hussein MZ, Al Ali SH, Zainal Z, Hakim MN. Development of antiproliferative nanohybrid compound with controlled release property using ellagic acid as the active agent. International Journal of Nanomedicine. 2011;6(1):1373–1383. Available:http://doi:10.2147/IJN.S21567
38. Xiong G, Luo L, Li C, Yang X. Synthesis of mesoporous ZnO (m-ZnO) and catalytic performance of the Pd/m-ZnO catalyst for methanol steam reforming. Energy & Fuels. 2009;23(3):1342–1346. Available:http://doi:10.1021/ef8008376
39. Dhamodharan P, Gobi R, Shanmugam N, Kannadasan N, Poonguzhali R, Ramya S. Synthesis and characterization of surfactants assisted Cu^{2+}doped ZnO nanocrystals. Spectrochimica Acta Part A: Molecular and Biomolecular Spectroscopy. 2014;131:125–131. doi.org/10.1016/j.saa.2014.04.083.
40. Modwi A, Abbo MA, Hassan EA, Ammar Houas. Adsorption kinetic and photocatalytic degradation of malachite green (MG) via Cu/ZnO nanocomposites. Journal of Environmental Chemical Engineering. 2017;5:5954–5960. doi.org/10.1016/j.jece.2017.11.024
41. Jongnavakit P, Amornpitoksuk P, Suwanboon S, Ndiege N. Preparation and photocatalytic activity of Cu-doped ZnO thin films prepared by the sol–gel method. Appl. Surf. Sci. 2012;258:8192–8198. doi.org/10.1016/j.apsusc.2012.05.021
42. Ghiloufi I, Ghoul J. El, Modwi A, Mir L. El. Ga-doped ZnO for adsorption of heavy metals from aqueous solution. Materials Science in Semiconductor Processing. 2016;42(3):102–106. Available:http://doi:10.1016/j.mssp.2015.08.047
43. Oskoei V, Dehghani MH, Nazmara S, Heibati B, Asif M, Tyagi I, Gupta VK. Removal of humic acid from aqueous solution using UV/ZnO nano-photocatalysis and adsorption. Journal of Molecular Liquids. 2015;213:374–380. Available:http://doi:10.1016/j.molliq.2015.07.052
44. Ayeshamariam A, et al. Synthesis and characterization of ZnO–CuO nanocomposites powder by modified perfume spray pyrolysis method and its antimicrobial investigation. Journal of Semiconductors. 2018;39(3):033001. Available:http://doi:10.1088/1674-4926/39/3/033001
45. Kaviyarasu K, et al. Synthesis and characterization studies of MgO: CuO nanocrystals by wet-chemical method. Spectrochimica Acta Part A: Molecular and Biomolecular Spectroscopy. 2015;142: 405-409. Available:https://doi.org/10.1016/j.saa.2015.01.111
46. Subba Reddy Y, et al. Equilibrium and kinetic studies of the adsorption of acid blue 9 and Safranin O from aqueous solutions by MgO decked FLG coated Fuller's earth. Journal of Physics and Chemistry of Solids. 2018;123:43-51. Available:https://doi.org/10.1016/j.jpcs.2018.07.009
47. Lee HJ, Kim BS, Cho CR, Jeong SY. A study of magnetic and optical properties of Cu doped ZnO. Phys. Stat. Sol. 2004; 241(7):1533-1536. Available:https://doi.org/10.1002/pssb.200304614
48. Jongnavakit P, Amornpitoksuk P, Suwanboon S, Ndiege N. "Preparation and photocatalytic activity of Cu-doped ZnO

thin films prepared by the sol–gel method. Applied Surface Science. 2012;258(20): 8192–8198.
Available:https://doi:10.1016/j.apsusc.2012.05.021

49. Chauhan, Kumar A, Chaudhary RP. Structure and optical properties of $Zn_{1-X}Ni_X O$ nanoparticles by coprecipitation methodruby. Journal of Optoelectronics and Biomedical Materials. 2011;3(1):17-23.
Available:https://10.1007/s11164-011-0478-5
50. Furdyna JK. Diluted magnetic semiconductors. Appl. Phys. 1988;64(4).
Available:https://10.1063/1.341700
51. Zhang Y, Lin B, Fu Z, Liu C, Han W. Strong ultraviolet emission and rectifying behaviour of nanocrystalline ZnO films. Opt. Mater. 2006;28,1192–1196.
Available:https://doi:10.1016/j.optmat.2005.08.016
52. Gandhi V, Ganesan R, Hameed H, Syedahamed A, Thaiyan M. J. Phys. Chem. C. 2014;118:9715–9725.
53. Li P, Wang S, Li J, Wei Y. Structural and optical properties of Co- doped ZnO nanocrystallites prepared by a one-step solution route. Journal of Luminescence. 2012;132(1):220–225.
Available:http://doi:10.1016/j.jlumin.2011.08.019
54. Xu DH, Shen WZ. Cu-doped ZnO hemispherical shell structures: Synthesis and room-temperature ferromagnetism properties. Journal of Physical Chemistry C. 2012;116(24):13368–13373.
Available:http://doi:10.1021/jp3003849
55. Udayabhaskar R, Mangalaraja RV, Karthikeyan B. Thermal annealing induced structural and optical properties of Ca doped ZnO nanoparticles. Journal of Materials Science: Materials in Electronics. 2013;1–6.
Available:http://doi:10.1007/s10854-013-1225-z
56. Zotov AO, et al. Electrical conductivity of Cu/ZnO/Si heterostructures. IOP Conf. Series: Journal of Physics: Conf. Series. 2017;816:012013.
Available:https://10.1088/1742-6596/816/1/012013

Peer-review history:
The peer review history for this paper can be accessed here:
http://www.sdiarticle3.com/review-history/47734